Invariant theory and orientational phase transitions

Joseph Rudnick[1,*] and Robijn Bruinsma[1,2,†]

[1]*Department of Physics and Astronomy, University of California, Los Angeles, California 90095, USA*
[2]*Department of Chemistry and Biochemistry, University of California, Los Angeles, California 90095, USA*

The Landau theory of phase transitions has been productively applied to phase transitions that involve rotational symmetry breaking, such as the transition from an isotropic fluid to a nematic liquid crystal. It even can be applied to the orientational symmetry breaking of simple atomic or molecular clusters that are not true phase transitions. In this paper, we address fundamental problems that arise with the Landau theory when it is applied to rotational symmetry breaking transitions of more complex particle clusters that involve order parameters characterized by larger values of the l index of the dominant spherical harmonic that describes the broken symmetry state. The problems are twofold. First, one may encounter a thermodynamic instability of the expected ground state with respect to states with lower symmetry. A second problem concerns the proliferation of quartic invariants that may or may not be physical. We show that the combination of a geometrical method based on the analysis of the space of invariants, developed by Kim to study symmetry breaking of the Higgs potential, with modern visualization tools provides a resolution to these problems. The approach is applied to the outcome of numerical simulations of particle ordering on a spherical surface and to the ordering of protein shells.

I. INTRODUCTION

The freezing of fluids has fascinated generations of scientists. When temperature is lowered, interacting atoms and molecules can transform spontaneously from a shapeless, entropy-dominated fluid into an ordered crystal that has a well-defined, faceted shape. The ordering transition involves a loss of symmetry: An extended fluid is symmetric with respect to any translation or rotation but as a crystal, this same system is symmetric only with respect to a discrete set of translations and rotations. Spontaneous symmetry breaking of this type is not restricted to the phase transitions of extended or bulk systems. When a nanometer-sized cluster of atoms freezes, it also can adopt an ordered state with reduced symmetry [1]. An important difference between the freezing of bulk liquids and that of particle clusters is that the freezing of a particle cluster cannot be a true phase transition because it only involves a small, finite system. Nevertheless, an extended system of interacting atomic clusters—a possible model of a glass—still can exhibit a genuine phase transition of this type [2].

Another important difference is that a cluster of atoms in the liquid state has full rotational symmetry but no translational symmetry. The symmetry group of a cluster in the liquid state typically is O(3), the group of all rotations and reflections, or the group of all rotations SO(3) in the case of chiral molecules. Neither the ordered nor the disordered cluster has any form of translational symmetry. Rotational symmetry breaking without translational symmetry breaking is encountered as well in extended systems, such as the transition from an isotropic fluid to a nematic liquid crystal with broken orientational symmetry [3]. In an important pa-

per, Steinhardt, Nelson, and Ronchetti [2] (SNR) proposed that a version of the Landau theory for orientational phase transitions of liquid crystals could be applied to the freezing of particle clusters. The order parameter was the radially averaged angle-dependent density $\rho(\Omega)$ of the cluster, with Ω being a solid angle measured from the center of a cluster of atoms or molecules. This density is then expanded in series of spherical harmonics:

$$\rho(\Omega) = \sum_{l=0}^{\infty} \sum_{m=-l}^{l} c_{l,m} Y_l^m(\Omega). \tag{1.1}$$

Under the symmetry operations of O(3), each set of $2l + 1$ expansion coefficients $c_{l,m}$ in this series transforms as an irreducible representation of O(3). One of the principles of the Landau theory of phase-transition states that continuous or near-continuous symmetry-breaking transitions should be associated with just one irreducible representation of the symmetry group of the high-symmetry phase, so just one particular value of l should characterize spontaneous orientational symmetry breaking. The set of $2l + 1$ expansion coefficients $c_{l,m}$ associated with that l value is then the *primary order parameter* of the transition. For example, the onset of orientational order in nematic and cholesteric liquid crystals are associated by $l = 2$, with various combinations of the azimuthal quantum number m. Irreducible representations with different l values may well be "entrained" by the primary order parameter through nonlinear terms in the free energy but these play only a limited role, so the associated $c_{l,m}$ are known as secondary order parameters. SNR proposed that the ordering of small particle clusters is dominated by an $l = 6$ state with icosahedral symmetry. This was based on the construction of a variational free energy in the form of a functional $F([\rho(\Omega)])$ expressed in terms of the $c_{l,m}$. Such a variational free energy has to transform as a scalar under

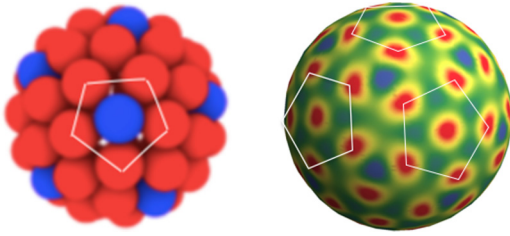*jarudnick@physics.ucla.edu
†bruinsma@physics.ucla.edu

FIG. 1. Left: Icosahedral state of $N = 72$ Lennard-Jones particles on a sphere (from Ref. [4]). Right: the $l = 16$ icosahedral spherical harmonic with 72 maxima (from Ref. [5]).

the symmetry operations of O(3) of the disordered state. This is achieved by constructing $F([\rho(\Omega)])$ from sums of combinations of $c_{l,m}$ that transform individually as invariants under O(3) or SO(3).

The focus of the present article is on orientational ordering transitions with l values larger than 6. Numerical simulations of 72 particles on a spherical surface interacting via a Lennard-Jones potential reported that there were various competing forms of orientational ordering [4]. The example shown in Fig. 1 (left), has icosahedral symmetry. Icosahedral states can be constructed from certain linear combinations of spherical harmonics known as *icosahedral spherical harmonics*, though only for certain values of l. The $l = 16$ icosahedral spherical harmonic has 72 maxima, as shown in Fig. 1, right, so it could serve as the primary order parameter for the icosahedral ordering of 72 particles on a spherical surface. A second case is provided in the work of Lorman and Rochal [6], who systematically compared the surface densities of icosahedral viral capsids with the icosahedral spherical harmonics. An example is shown in Fig. 2 where the capsid of the canine parvovirus, which is composed of 60 identical proteins, is compared with the $l = 15$ icosahedral spherical harmonic, which also has 60 maxima. The parvovirus belongs to the smallest class of icosahedral viruses. Larger viral capsids correspond to icosahedral spherical harmonic values of l that are larger than 15 [6,8]. Since transitions from disordered to ordered viral capsids have been observed experimentally [9], one could ask whether such transitions can be described by SNR-type Landau theories.

Fundamental problems are encountered if one attempts to directly extend SNR to larger values of l. The first problem concerns thermodynamic stability. The simulations for
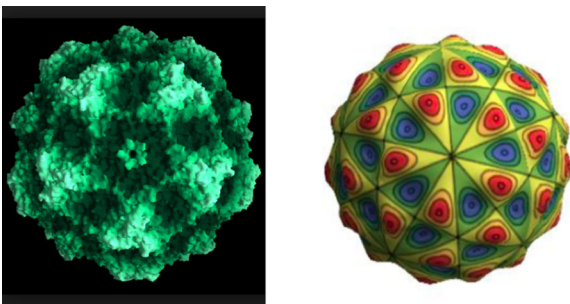

FIG. 2. Left: Capsid of the canine parvovirus, as reconstructed by x-ray diffraction (from Ref. [7]). It is composed of 60 identical proteins placed in an icosahedral pattern. Right: The $l = 15$ icosahedral spherical harmonic with 60 maxima (from Ref. [5]).

72 particles on a spherical surface and the observations on the parvovirus seem to indicate that icosahedral shells that have a primary order parameter that transforms either as an $l = 16$ or as an $l = 15$ icosahedral spherical harmonic should be thermodynamically stable for some appropriate choice of thermodynamic system parameters. However, when the $l = 15$ and $l = 16$ cases were investigated, states with icosahedral symmetry turned out to be thermodynamically unstable [5,10]. Separately, Matthews [11] found that rotational symmetry breaking in the $l = 16$ sector produces states with *tetrahedral* symmetry. Strangely, the thermodynamic stability of the $l = 15$ icosahedral state could be restored by mixing in small amounts of $l = 16$ [5,10]. The fact that icosahedral symmetry appears to be associated with a *mixed $l = 15 + 16$* state is unsatisfactory from the viewpoint of Landau theory because it seems to associate rotational symmetry breaking with *two* irreducible representations of the symmetry group of the uniform state. Note that the $l = 16$ contribution could not be viewed in this case as a secondary order parameter since secondary order parameters should not determine the stability of the primary order parameter.

A second issue concerns the number of invariants that are to be included in the Landau variational free energy. SNR effectively included two invariants for $l = 6$ (one cubic and one quartic) but Jarić [12,13] showed that there are actually three independent quartic invariants for $l = 6$. Depending on the coefficients of these three invariants, the $l = 6$ icosahedral state may or may not be the ground state. We will see that the number of independent quartic invariants increases in a stepwise linear fashion with l and that these new invariants in general are *nonlocal*. Do all these nonlocal invariants really have to be included even if the underlying physical system itself only involves short-range interactions? We will show that these two issues are actually intimately connected.

To analyze this confusing state of affairs, we apply in this article a geometrical method that was developed by Kim [14] in the context of symmetry breaking of the Higgs potential. This method starts from a vector space spanned by a set of linearly independent invariants constructed from the order parameter. By letting the order parameter range over all possible values, a volume is generated in the invariant space. This "Kim volume" is a purely mathematical construct that is independent of the parameters of the physical system. For the present case, the invariants are polynomial expressions of the $c_{l,m}$ parameters in Eq. (1.1). A schematic example of a Kim plot is shown in Fig. 3 for the case of three invariants λ_{1-3}. Next, families of constant free-energy hypersurfaces are constructed by allowing the physical parameters to vary. A broken symmetry state is associated with a point where such a constant free-energy surface touches the Kim volume.[1]

In Sec. II, we show how these invariants can be constructed systematically in terms of the $c_{l,m}$ parameters. Next, we practice with the Kim method for the simpler cases of $l = 2, l = 6$, and $l = 7$. In Sec. III, we apply this method to orientational ordering in the $l = 15$ sector, the $l = 16$ sector, and the

---

[1]To be precise, we will generalize the approach of Kim, which applies in its standard form to a free energy, or effective Hamiltonian, with only quadratic and quartic, but no cubic, contributions.
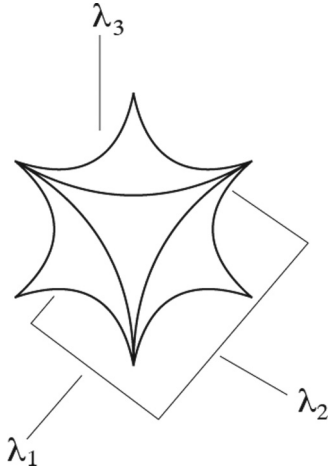
FIG. 3. Three-dimensional space of invariants. The surface encloses the set of points generated when the order-parameter set $Q_{L,M}$ varies over its allowed values. The plane represents a surface of constant free energy. Intersection of the plane with the surface corresponds to a state with broken symmetry (from Ref. [14]).

combined $l = 15 + 16$ sector. The fact that the icosahedral state is unstable in the pure $l = 15$ sector and largely unstable in the pure $l = 16$ sector is confirmed in full generality for variational free energies with local invariants. We also confirm that stable icosahedral states appear in the mixed $l = 15 + 16$ sector. Finally, we show that the principles of Landau theory can be "saved" if one includes the nonlocal invariants, at least for the case of the $l = 15$ sector. Using diagrammatic perturbation theory, we show that the nonlocal invariants are generated *from a purely local variational free energy* when one integrates out the $l \neq 15$ sectors. At least formally, an orientational symmetry breaking transition from an isotropic to an $l = 15$ icosahedral state can be constructed within the $l = 15$ sector—including the thin sliver of intervening tetrahedral states that was noted in the earlier numerical work—using a Kim construction with nonlocal invariants. More generally, a mixed $l = 15 + 16$ representation provides an economical description of such transitions.

II. INVARIANTS AND THE KIM METHOD

In this section, we lay the mathematical groundwork. We first demonstrate a systematic construction method to obtain the independent invariants for given l based on the *Wigner 3-j* symbols. The method generalizes that of Ref. [12] for the $l = 6$ case. Next, we construct Landau free energies, in the form of sums of invariants, up to quartic order for the $l = 2$, $l = 6$, and $l = 7$ cases. The $l = 6$ case will be the prototype of a discontinuous orientational ordering transition that is, from the viewpoint of the Kim method [14], nontrivial while the $l = 7$ case will be the prototype of a nontrivial continuous orientational ordering transition. Finally, we demonstrate how the Kim geometrical method ("Kim construction") works for these prototypes.

A. Construction of invariants

A square-integrable function defined on the surface of a sphere, such as the mass density $\rho(\theta, \phi)$, can be expanded
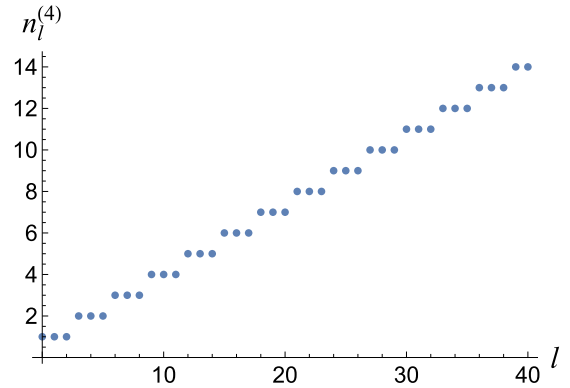

FIG. 4. The number of distinct quartic terms, $n_l^{(4)}$, plotted for l ranging from 0 to 40. See Appendix B, Eq. (B3).

in a spherical harmonics series in the form $\rho(\theta, \phi) = \sum_{l=0}^{\infty} \sum_{m=-l}^{l} c_{l,m} Y_l^m(\theta, \phi)$. If the scalar quantity of interest is to be real (as will be the case throughout this article), then $c_{l,m} = (-1)^m c_{l,-m}^*$. When we write the expansion as

$$\rho(\theta, \phi) = \sum_{l=0}^{\infty} \sum_{m=-l}^{l} \rho_{l,m}(\theta, \phi) = \sum_{l=0}^{\infty} \rho_l(\theta, \phi), \qquad (2.1)$$

then $\rho_{l,-m}$ is the complex conjugate of $\rho_{l,m}$ and ρ_l is real.

When we turn to the Landau variational free energy for the density, if the expansion in powers of $c_{l,m}$ parameters is limited to terms no higher than fourth order and confined to a single value of l, then the most general form of the free energy $\mathcal{F}_l$ is

$$\mathcal{F}_l = \sum_{k=2}^{4} \sum_{n=1}^{n_l^{(k)}} f_{k,n} I_n^{(k,l)}. \qquad (2.2)$$

Here, $n_l^{(k)}$ is the number of independent kth-order invariant polynomials in the $c_{l,m}$ parameters for the l value in question. Its value is determined by the Molien polynomial [15]. Next, $I_n^{(k,l)}$ is the nth invariant polynomial, a system-independent mathematical construct. Finally, the expansion coefficients $f_{k,n}$ depend on the thermodynamic parameters of the particular physical system in question. As discussed further in the Supplemental Material [16], the expansion coefficients $t_l/2 = f_{2,1}$ of the $k = 2$ quadratic invariant can be related to two-point correlation functions of the system such as the linear susceptibility, the static structure factor, and the pair distribution function. For convenience, we will refer to t_l as the "reduced temperature" of the system.

We demonstrate in Appendix A that, for any value of l, there is only one quadratic invariant, namely the integral $I^{(2,l)} = \int \rho_l(\theta, \phi)^2 \sin \theta \, d\theta d\phi$. There also is at most one cubic invariant $I^{(3,l)} = \int \rho_l(\theta, \phi)^3 \sin \theta \, d\theta d\phi$ for even values of l and none for odd l values. By contrast, using heuristic arguments we show in Appendix B that the number $n_l^{(4)}$ of independent quartic invariants rises in a stepwise linear manner with l, as shown in Fig. 4 (note the triplet grouping). Two of the quartic invariants are straightforward. They are obtained, respectively, from the integral of the fourth power of $\rho_l(\theta, \phi)$ and the square of the quadratic invariant (A8). We term the first invariant the *local* quartic invariant and the

second the *trivial* quartic invariant, which is nonlocal. For $l = 0, 1$, and 2, those two quartic invariants are identical to within an overall multiplicative constant while for $l \geqslant 3$ the two invariants differ in form [see Fig. 4 and Appendix B, Eq. (B3)].

One can systematically construct the fourth-order invariants using the following quantity as a building block [12]:

$$
\mathcal{V}(l_1, m_1, l_2, m_2, l_3, m_3)
$$
$$
= \int Y_{l_1}^{m_1}(\theta, \phi) Y_{l_2}^{m_2}(\theta, \phi) Y_{l_3}^{m_3}(\theta, \phi) \sin \theta \, d\theta d\phi
$$
$$
= \sqrt{\frac{(2l_1 + 1)(2l_2 + 1)(2l_3 + 1)}{4\pi}} \begin{pmatrix} l_1 & l_2 & l_3 \\ 0 & 0 & 0 \end{pmatrix}
$$
$$
\times \begin{pmatrix} l_1 & l_2 & l_3 \\ m_1 & m_2 & m_3 \end{pmatrix}. \tag{2.3}
$$

The terms in brackets are Wigner $3j$ symbols [17]. For example, the cubic expression

$$
\sum_{m_1, m_2, m_3 = -l}^{l} \mathcal{V}(l, m_1, l, m_2, l, m_3) c_{l, m_1} c_{l, m_2} c_{l, m_3} \delta_{m_1 + m_2 + m_3} \tag{2.4}
$$

is the invariant under rotation that is proportional to the local cubic invariant $\int \rho_l(\theta, \phi)^3 \sin \theta \, d\theta d\phi$. Next, the fourth-order local invariant, arising from the integral of the fourth power of the density $\rho_l(\theta, \phi)$ over the surface of the sphere, can be expressed in terms of the Wigner $3j$ symbols as

$$
\sum_{j=0}^{2l} \sum_{m_1, m_2, m_3, m_4 = -l}^{l} (-1)^{m_1 + m_2} \mathcal{V}(l, m_1, l, m_2, j, -m_1 - m_2)
$$
$$
\times \mathcal{V}(l, m_3, l, m_4, j, -m_3 - m_4) c_{l, m_1} c_{l, m_2} c_{l, m_3} c_{l, m_4}
$$
$$
\times \delta_{m_1 + m_2 + m_3 + m_4}. \tag{2.5}
$$

Both (2.4) and (2.5) can be depicted graphically. Figure 5(a) shows the graphical element for $\mathcal{V}(l_1, m_1, l_2, m_2, l_3, m_3)$, while Fig. 5(b) depicts the combination of $\mathcal{V}$'s in (2.5). Not all values of j contribute to the summation over the internal line: For odd values of j, the expression evaluates to zero.

Figure 5(b) provides a clue as to how additional quartic invariants could be generated: The individual terms in the summation of the internal line over different j each are *separately* rotational invariants. The reason is that a rotation of the sphere in 3-space in general scrambles the $2l + 1$ coefficients $c_{l,m}$ when the z axis is rotated. However, such a rotation cannot mix $c_{l,m}$ coefficients with $c_{l',m'}$ coefficients when $l' \neq l$, since they belong to different irreducible representations. Similarly, rotations will not scramble the different j terms in the summation. The new terms can be graphically represented as shown in Fig. 5(c). It is easy to check that the $j = 0$ term corresponds to the trivial invariant.

It might seem that this method provides a scheme to construct *infinitely many* quartic invariants for all even j, though we know that these invariants cannot be all independent. First, j and the two l's must satisfy the triangle inequalities: $0 \leqslant j \leqslant 2l$. For a given l, start from $j = 0$ and recall that the trivial quartic invariant is separate from the local quartic invariant for $l \geqslant 3$. Next, go to the $j = 2$ case and check if this generates an independent invariant, which is the case for
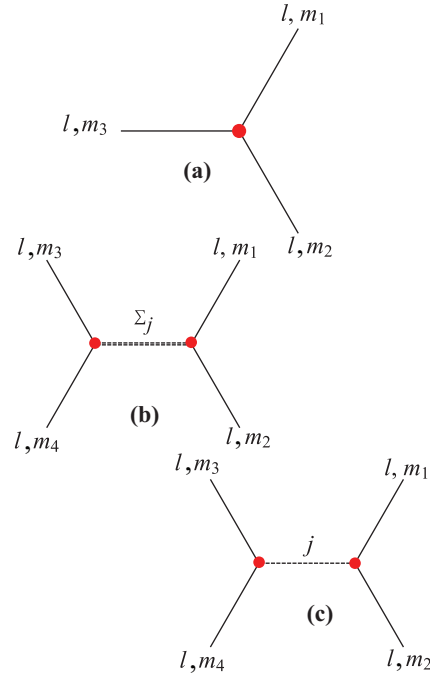

FIG. 5. Diagrams useful in the evaluation of third-order and quartic vertices. (a) Graphical representation of the quantity $\mathcal{V}(l_1, m_1, l_2, m_2, l_3, m_3)$, as defined in (2.3). (b) Graphical representation of the product $\sum_j \mathcal{V}(l, m_1, l, m_2, j, -m_1 - m_2)$ $\mathcal{V}(l, m_3, l, m_4, j, -m_3 - m_4)(-1)^{m_1 + m_2}$ in (2.5). The double-dashed line expresses the fact that the overall index j carried by that line is summed over. (c) Graphical representation of a quartic invariant generated from the third-order vertex in panel (a), mediated by a single value of j. This diagram corresponds to the expression $\mathcal{V}(l, m_1, l, m_2, j, -m_1 - m_2) \mathcal{V}(l, m_3, l, m_4, j, -m_3 - m_4)(-1)^{m_1 + m_2}$, the intermediate value of j having been fixed.

$l \geqslant 6$ (see Appendix B). This suggests a pattern and one can indeed repeat this for any even j until $j = 2l$ after which no more invariants are generated. For all values of l that we checked, this method produces the full number of independent invariants that is imposed by the Molien polynomial.

The nonlocal invariants also can be viewed as being generated from the expression

$$
\int d\theta d\phi \int d\theta' d\phi' [\rho(\theta, \phi)^2 \mathcal{K}_j(\theta, \phi, \theta' \phi') \rho(\theta', \phi')^2], \tag{2.6}
$$

where

$$
\mathcal{K}_j(\theta, \phi, \theta' \phi') = \sum_{m=-j}^{j} Y_j^m(\theta, \phi) Y_j^m(\theta', \phi')^*, \tag{2.7}
$$

which, by inspection, is a rotational invariant for any j. The new invariants are produced by replacing the squared scalar densities with ρ_l^2. The graphical representation of this term is reminiscent of a Feynman diagram for the interaction between two particles mediated by the exchange of a mode with "propagator" $\mathcal{K}_j$ so we will call these "mediated invariants." In the Supplemental Material [16], we discuss how nonlocal invariants can be generated by coupling the density profile ρ to a harmonic scalar field such as the *shape profile* associated with variation of the sphere radius. The mediated invariants

appear after the shape variables are integrated over. The coefficients of the mediated quartic invariants produced in this manner are always negative.

To recapitulate: the Landau free energy with invariants up to quartic order constructed from a single value of l has only one quadratic invariant, obtained by integrating the square of the relevant density, $\rho_l(\theta, \phi)$, over the surface of the sphere. Next, it has at most one cubic invariant, obtained in the same way from the cube of $\rho_l(\theta, \phi)$, or alternatively from Wigner $3j$ symbols via (2.4); when l is odd, the cubic invariant evaluates to zero. Quartic invariants will vary in number, depending on the value of l, but there is always the local invariant, obtained by integrating $\rho_l(\theta, \phi)^4$ over the surface of the sphere, and the trivial invariant, obtained by squaring the quadratic invariant. From $l = 0$ to $l = 2$, those two invariants are identical to within a multiplicative constant. For $l = 6$ and above, there are additional, mediated, quartic invariants, which can be obtained via the approach illustrated in Fig. 5(c), up to the required number shown in Fig. 4.

B. Landau variational energies for $l = 2$, $l = 6$, and $l = 7$

Having in hand a systematic construction method for the invariants, we are now in a position to construct Landau energies for specific cases.

1. Landau energy for $l = 2$

We start with $l = 2$, which is realized by the familiar case of nematic ordering in liquid crystals [3]. We will reformulate the standard treatment in a manner that brings out the connection with the Kim method. Configuration space is five-dimensional for $l = 2$. Imposing the condition that the density is real leads to the relations

$$c_{2,-2} = r_1 + is_1, \tag{2.8}$$

$$c_{2,-1} = r_2 + is_2, \tag{2.9}$$

$$c_{2,0} = \sqrt{2}r_3, \tag{2.10}$$

$$c_{2,1} = -(r_2 - is_2), \tag{2.11}$$

$$c_{2,2} = r_1 - is_1, \tag{2.12}$$

where the r_i's and the s_l's are real numbers. This parametrization is readily generalized to arbitrary values of l. In terms of these variables, the quadratic invariant has the form

$$\langle \rho_2^2 \rangle = \int \rho_2(\theta, \phi)^2 \sin \theta \, d\theta \, d\phi$$

$$= \sum_{m=-2}^{2} c_{2,m} c_{2,-m} (-1)^m$$

$$= 2\left(r_1^2 + r_2^2 + r_3^2 + s_1^2 + s_2^2\right). \tag{2.13}$$

Next, we construct a linear, five-dimensional vector space ("configuration space") from the five variables r_i and s_k, with five-component vectors defined as

$$\begin{pmatrix} r_2 \\ r_2 \\ r_3 \\ s_1 \\ s_2 \end{pmatrix}. \tag{2.14}$$

The quadratic form on the right-hand side of (2.13), the square of the modulus of the five-component vectors, corresponds to the unique quadratic invariant under rotations in configuration space. As is well known, infinitesimal rotations in three-dimensional space ("Euclidean space") are generated by three 3-by-3 antisymmetric matrices. There are three 5-by-5 matrices in configuration space that correspond to the three generators in Euclidean space:

x axis:

$$\begin{pmatrix} 0 & 0 & 0 & 0 & 1 \\ 0 & 0 & 0 & 1 & 0 \\ 0 & 0 & 0 & 0 & \sqrt{3} \\ 0 & -1 & 0 & 0 & 0 \\ -1 & 0 & -\sqrt{3} & 0 & 0 \end{pmatrix}, \tag{2.15}$$

y axis:

$$\begin{pmatrix} 0 & -1 & 0 & 0 & 0 \\ 1 & 0 & -\sqrt{3} & 0 & 0 \\ 0 & \sqrt{3} & 0 & 0 & 0 \\ 0 & 0 & 0 & 0 & -1 \\ 0 & 0 & 0 & 1 & 0 \end{pmatrix}, \tag{2.16}$$

and z axis:

$$\begin{pmatrix} 0 & 0 & 0 & 2 & 0 \\ 0 & 0 & 0 & 0 & 1 \\ 0 & 0 & 0 & 0 & 0 \\ -2 & 0 & 0 & 0 & 0 \\ 0 & -1 & 0 & 0 & 0 \end{pmatrix}. \tag{2.17}$$

Since these are antisymmetric, it follows that an infinitesimal rotation in Euclidean space generates an infinitesimal rotation in configuration space. Similarly, finite rotations in Euclidean space generate finite rotations in configuration space. Next, in terms of the real expansion coefficients, the single cubic invariant is

$$\langle \rho_2^3 \rangle = \int \rho_2(\theta, \phi)^3 \sin \theta \, d\theta \, d\phi$$

$$= -\frac{6}{7}\sqrt{\frac{10}{\pi}}r_3 s_1^2 + \frac{3}{7}\sqrt{\frac{10}{\pi}}r_3 s_2^2 - \frac{3}{7}\sqrt{\frac{30}{\pi}}r_1 s_2^2$$

$$+ \frac{6}{7}\sqrt{\frac{30}{\pi}}r_2 s_1 s_2 + \frac{2}{7}\sqrt{\frac{10}{\pi}}r_3^3 - \frac{6}{7}\sqrt{\frac{10}{\pi}}r_1^2 r_3$$

$$+ \frac{3}{7}\sqrt{\frac{10}{\pi}}r_2^2 r_3 + \frac{3}{7}\sqrt{\frac{30}{\pi}}r_1 r_2^2. \tag{2.18}$$

This expression is *not* invariant under general rotations in configuration space though—by construction—it still is an invariant under rotations in Euclidean space. Finally, the unique fourth-order term

$$\langle \rho_2^4 \rangle = \frac{15\left(r_1^2 + r_2^2 + r_3^2 + s_1^2 + s_2^2\right)^2}{7\pi} \tag{2.19}$$

is invariant under rotations in both Euclidean and configuration space.

Define spherical coordinates in configuration space with A being the modulus and with the four angular variables ψ_k's, with $k = 1, 2, 3, 4$, determining direction in configuration space. In these coordinates, the $l = 2$ Landau free energy has,

up to fourth order, the general form

$$\mathcal{F}_2(A, \psi_k) = \frac{t_2}{2}A^2 + \frac{u}{3}A^3 Q_3(\{\psi_k\}) + \frac{v}{4}A^4. \quad (2.20)$$

The system parameters t_2, u, and v incorporate information about the physics of the particular system in question while $Q_3(\{\psi_k\}) = \langle\rho_2^3\rangle/A^3$ is a combination of trigonometric functions of the four angles ψ_k that is universal in the sense that it does not depend on the system parameters.

Fix the set of angles $\{\psi_k\}$ and decrease t_2, starting from a large, positive value. For large and positive t_2, the only solution of the equation $\frac{\partial\mathcal{F}(A,\{\psi_k\})}{\partial A} = 0$ is $A = 0$, which is the symmetric state with $\mathcal{F}_2(A = 0, \{\psi_k\}) = 0$. The transition temperature $t_c(\{\psi_k\})$ for the first-order phase transition is obtained by demanding that the pair of equations $\mathcal{F}_2(A, \{\psi_k\}) = 0$ and $\frac{\partial\mathcal{F}_2(A,\{\psi_k\})}{\partial A} = 0$ has a nontrivial solution. Eliminating A gives an expression for the transition temperature in terms of the direction in configuration space:

$$2t_c(\{\psi_k\}) = \frac{u^2}{v}[Q_3(\{\psi_k\})]^2. \quad (2.21)$$

The equation marks the rotational symmetry breaking transition, along a particular direction in configuration space. Now, allow the set of angles $\{\psi_k\}$ to vary. Symmetry breaking takes place *at the highest possible value* of $t_c(\{\psi_k\})$. The determination of the prevailing symmetry for orientational ordering in the $l = 2$ sector is reduced to the purely mathematical question of determining the maximum of the modulus of the universal expression $Q_3(\{\psi_k\})$ in configuration space. Numerical minimization of $|Q_3|$ is straightforward. Only r_3 is nonzero at the maximum of $|Q_3|$, which corresponds to the expected $l = 2$, $m = 0$ nematic state for the case of liquid crystals.[2]

2. Landau energy for $l = 6$

Next we turn to $l = 6$, the case explored by SNR. For $l = 6$, configuration space expands to $12 + 1 = 13$ dimensions. There is, as always, only one quadratic and one cubic invariant, but now there are three quartic invariants: the trivial invariant, the local invariant, and the $j = 2$ mediated invariant—or, equivalently, any three independent linear combinations of those three invariants. It is instructive to start by first including only the local quartic invariant $Q_{4,1}$. Following the same steps as for $l = 2$, the variational energy is

$$\mathcal{F}_6 = t_6 A^2 + \frac{u}{3}A^3 Q_3(\{\psi_i\}) + \frac{v}{4}A^4 Q_{4,1}(\{\psi_i\}), \quad (2.22)$$

where the set $\{\psi_i\}$ refers to the 12 angular variables that collectively define a direction in the 13-dimensional configuration space. Next, apply the method we used to determine the transition temperature for $l = 2$, i.e., set the derivative with respect to A to zero for a fixed set of angles $\{\psi_i\}$

$$\begin{aligned} 0 &= \frac{\partial\mathcal{F}_6}{\partial A} \\ &= A[2t_6 + uAQ_3(\{\psi_i\}) + vA^2 Q_{4,1}(\{\psi_i\})] \end{aligned} \quad (2.23)$$

and then demand that at the transition point the free energy itself must be zero:

$$\begin{aligned} 0 &= \mathcal{F}_6 \\ &= A^2\left[t + \frac{u}{3}AQ_3(\{\psi_i\}) + \frac{v}{4}A^2 Q_{4,1}(\{\psi_i\})\right]. \end{aligned} \quad (2.24)$$

Solving the the simultaneous equations (2.23) and (2.24), for t_6 and nonzero A, we find

$$t_6 = \frac{Q_3(\{\psi_i\})^2 u^2}{9 Q_{4,1}(\{\psi_i\})v}, \quad (2.25)$$

$$A = -\frac{2Q_3(\{\psi_i\})u}{3Q_{4,1}(\{\psi_i\})v}. \quad (2.26)$$

Now, as t_6 is lowered, ordering first occurs for those values of $\{\psi_i\}$ at which t_6 on the right-hand side of (2.22) takes on the largest value. This means that we must seek the maximum value of the ratio $Q_3(\{\psi_i\})^2/Q_4(\{\psi_i\})$ instead of the $l = 2$ criterion of maximizing the modulus of Q_3. The numerical effort required to maximize $Q_3(\{\psi_i\})^2/Q_4(\{\psi_i\})$ again is modest: The maximum corresponds to the $l = 6$ icosahedral spherical harmonic, in agreement with SNR. The transition is again first order.

Now include the $j = 2$ mediated quartic invariant and also the trivial nonlocal quartic invariant. The full $l = 6$ Landau free energy can be expressed as

$$\mathcal{F}_6 = \frac{t_6}{2}A^2 + \frac{u}{3}A^3 Q_3 + \frac{1}{4}A^4[aQ_{4,1} + bQ_{4,2} + c], \quad (2.27)$$

where the subscript 4,1 indicates the local quartic invariant and the subscript 4,2 is the $j = 2$ mediated quartic invariant. Next, $a(= v)$, b, and c are three system-dependent expansion coefficients. The coefficient c accounts here for the trivial invariant. Thermodynamic stability requires that only coefficients a, b, c are permitted such that for any set of angular variables the complete quartic term is positive. The transition temperature is

$$t_6 = \frac{u^2}{9}\frac{Q_3^2}{[aQ_{4,1} + bQ_{4,2} + c]} \quad (2.28)$$

(we suppressed here the dependence on the angular variables). The optimal direction in the 13-dimensional configuration space corresponds to the maximum of $Q_3^2/(aQ_{4,1} + bQ_{4,2} + c)$. Unlike the $l = 2$ case, numerical maximization is more complicated because the quantity to be maximized (t_6) now depends on the physical parameters a, b, and c.

3. Landau energy for $l = 7$

Unlike the $l = 2$ and $l = 6$ cases, $l = 7$ has no (as yet known) physical realization. However, it represents an important contrast when it is compared to the $l = 6$ case, in that there is no cubic invariant because l is odd. This means that an $l = 7$ orientational ordering transition will be continuous in Landau mean-field theory. Just as for $l = 6$, there are three independent quartic invariants: The local invariant, the trivial invariant, and the $j = 2$ mediated invariant. For $l = 7$, configuration space has 15 dimensions with 14 angular variables $\{\psi_k\}$ plus the modulus A. The Landau variational free

---

[2]Historically, maximizing the cubic invariant was the criterium proposed by Alexander and McTague [18] in their pioneering study of melting viewed as an orientational phase transition.

energy has, up to fourth order, the form

$$\mathcal{F}_7 = \frac{t_7}{2}A^2 + \frac{1}{4}A^4[aQ_{4,1}(\{\psi_k\}) + bQ_{4,2}(\{\psi_k\}) + c]. \quad (2.29)$$

The four coefficients $a, b, c,$ and t_7 are again system-dependent parameters while the expressions $Q_{4,1}(\{\psi_k\})$ and $Q_{4,2}(\{\psi_k\})$ are universal functions of the angular variables.

For any set of angular variables, the critical point for the continuous symmetry breaking transition is now $t_7 = 0$, which provides no information about the selection of the angular variables. However, for $t_7 < 0$, minimization of the free energy with respect to A leads to

$$t_7 + A[aQ_{4,1}(\{\psi_k\}) + bQ_{4,2}(\{\psi_k\}) + c] = 0. \quad (2.30)$$

The corresponding angle-dependent free energy is

$$\mathcal{F}_{\min}(\{\psi_k\}) = -\frac{t_7^2}{4[aQ_{4,1}(\{\psi_k\}) + bQ_{4,2}(\{\psi_k\}) + c]}. \quad (2.31)$$

Minimization of this expression with respect to the angle variables determines the broken symmetry state. This means that for $l = 7$ the broken symmetry must be determined by minimizing the positive quantity

$$\Lambda = aQ_{4,1}(\{\psi_k\}) + bQ_{4,2}(\{\psi_k\}) + c, \quad (2.32)$$

which is again dependent on the system parameters.

C. Kim constructions for $l = 6$ and $l = 7$

The Kim construction [14] can be used as a graphical method for performing the minimization of system-dependent quantities such as Λ and Q_3^2/Λ in a manner that reveals system-independent information about competing broken symmetry states. Here, we apply the method to the cases $l = 6$ and $l = 7$.

1. $l = 7$

We will start with $l = 7$, in which case we need to minimize Λ as defined in (2.32). Construct a two-dimensional invariant vector space with linear combinations of the two independent nontrivial quartic invariants $Q_{4,1}$ and $Q_{4,2}$ as coordinate axes. While any independent pair of combinations of $Q_{4,1}$ and $Q_{4,2}$ can be used as coordinate pairs, we found, by trial and error, that $X = Q_{4,1} + Q_{4,2}$ and $Y = Q_{4,2}$ with $\Lambda(X, Y) = a(X - Y) + bY + c$ was a convenient choice for revealing the structure of the Kim regions in a more readily observable fashion. The set of points in the X-Y plane for which $\Lambda(X, Y) = a(X - Y) + bY + c$ is constant is then a straight line. Let θ be the angle this line makes with the X axis. It is convenient to absorb an overall factor $v = \sqrt{a^2 + b^2}$ in Λ and express the line as

$$\Lambda(X, Y) = (X - X_0)\cos\theta + (Y - Y_0)\sin\theta. \quad (2.33)$$

Note that a change of the values of the parameters X_0 and Y_0 amounts to an affine translation of the lines that leaves angles unchanged.

Next, randomly sample the 14 angles $\{\psi_k\}$ in the 15-dimensional configuration space over the full range of
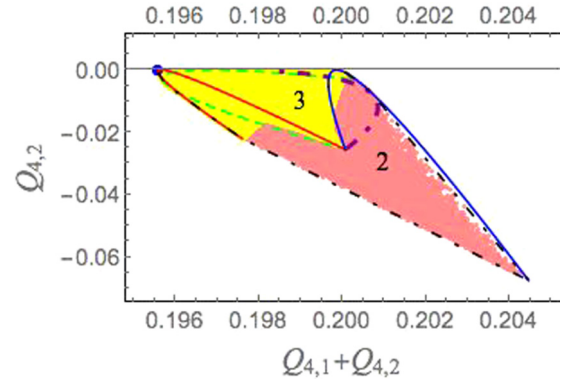

FIG. 6. Collection of allowed states for $l = 7$ in the X-Y plane where $X = Q_{4,1} + Q_{4,2}$ and $Y = Q_{4,2}$. Solid red curve in the upper left-hand portion of the plot, sixfold axis; green dashed curve adjacent to the red curve, fivefold axis; purple dashed curve in the upper right-hand portion, fourfold axis; blue curve skirting the right-hand boundary, sevenfold axis. The long and short dashed curves denote the boundary of the pink stippled twofold symmetry region; see Appendix C. The yellow region corresponds to threefold symmetry. Both regions are labeled with the corresponding symmetries. Finally, the blue solid dot on the upper left-hand corner is a point of tetrahedral symmetry.

mathematically allowed values.[3] This generates the colored area in the X-Y space shown in Fig. 6, which is a first example of a Kim plot. Note that this volume still is independent of the physical system parameters. Additional symmetries can be imposed that generate subsets of the Kim plot. For example, the darker, pink-colored area has twofold symmetry, and the lighter, yellow region corresponds to threefold symmetry. The demarcation between the two regions is somewhat misleading; the twofold symmetry region actually extends into the area covered by the threefold region (see Fig. 8). This is because there are instances of configurations with twofold symmetry that have precisely the invariants of a configuration with threefold symmetry. Clearly, there is not a one-to-one relationship between detailed order parameter structure and invariant values.

As described in the caption, the curves in the Kim plot correspond to the imposition of a four-, five-, six-, and sevenfold symmetry axis. Those curves meet at a point in the interior corresponding to C_∞ symmetry. Imposition of tetrahedral symmetry leads to a single point in the plot (blue dot in the upper left-hand corner). This means that tetrahedral symmetry corresponds to unique values of $Q_{4,1}$ and $Q_{4,2}$. Within our numerical precision, the blue dot lies on a sharp corner of the perimeter of the plot. Note that the $l = 7$ Kim plot gives the impression of being the projection of a surface from a higher dimensional space (as indeed it is).

The next step is the Kim construction. This involves, for $l = 7$, drawing lines of constant $\Lambda(X, Y)$ in the Kim plot with different lines corresponding to a different sets of physical system parameters. These are the surfaces of constant free

---

[3]In practice, we sample the parameters r_i and s_i, divided by the square root of the sum of their squares, e.g., $r_i/\sqrt{\sum_j r_j^2 + \sum_k s_k^2}$.
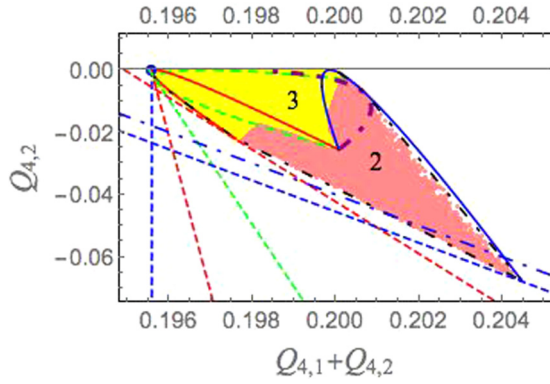
FIG. 7. Kim construction for $l = 7$. The dashed lines are lines of constant Λ that graze the Kim plot. They are drawn for increasing values of the system parameter θ, starting with the positively sloped dashed line for which $\theta = -0.01$. The point where it grazes the Kim plot has tetrahedral symmetry, indicated by the blue dot. The other lines, listed in increasing value of intercept with the horizontal, $Q_{4,1} + Q_{4,2}$, axis are the red dashed line, $\theta = 0.01$, corresponding to a sixfold axis; the green dashed line, $\theta = 0.05$, corresponding to a fivefold axis; another red dashed line, $\theta = 0.11$, again corresponding to a sixfold axis; and a blue dashed line, $\theta = 0.2$, corresponding to a sevenfold axis. Finally, the blue long-short-dashed line is parallel to the blue fivefold axis line and is associated with the same thermodynamic parameters, but with a larger value of Λ. This line intrudes into the interior of the Kim plot and passes through twofold symmetry states and a sevenfold symmetric density with a higher free energy.

energy referred to in the introduction. Examples are shown in Fig. 7 for the case that a is positive while b and c are negative. Recall that negative b and c can represent the physical case of coupling between density and an additional scalar field. The dashed lines in Fig. 7 are lines of constant Λ for different values of θ. The values of X_0 and Y_0 were—with the exception of the blue dash-dotted line—chosen so the constant Λ line is
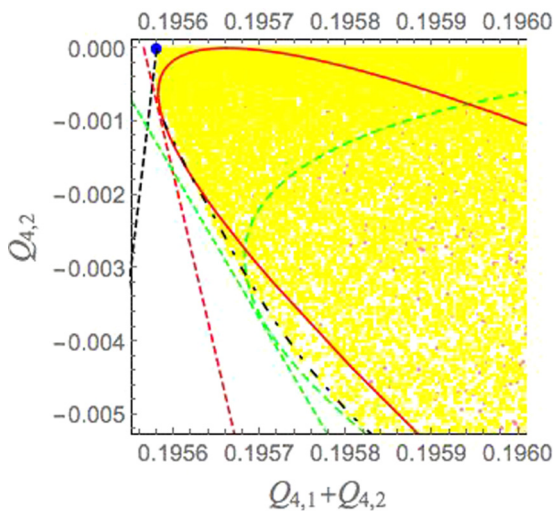

FIG. 8. Kim construction for the upper left-hand portion of the Kim plot shown in Fig. 7. The straight lines correspond to those shown in that figure. Note the darker pink stippling in the lighter threefold region, indicating that states with different order parameter structure can have the same invariant values.

FIG. 9. Phase plot for $l = 7$ for the case that the system parameter a is positive while b and c are negative. For increasing θ and t_7 negative, the system passes from a tetrahedral state to a state with a single sixfold symmetry axis, a fivefold axis, again a sixfold axis, and finally a sevenfold axis. The loci of the transition points are independent of t_7.

tangent to the Kim plot. Changing the values of X_0 and Y_0 for fixed θ amounts to a parallel shift of the line. Suppose the shift is such that the line lies entirely in the white region, for example by sliding the blue dashed line to the left without changing its slope. The value of Λ is reduced by this shift and this would lower the free energy, Eq. (2.31). However, symmetry breaking is not possible in this case since there is no set of allowed invariants corresponding to the set of angles ψ_i that are allowed along the line. We thus can disregard constant Λ lines that lie outside the Kim plot. Next, shift the blue dashed line to the right without changing its slope (so toward the blue dash-dotted line). The line enters the interior of the Kim plot. While the states along the dash-dotted line in the interior of the Kim plot are mathematically allowed broken symmetry states, they are *not* the minimum free-energy states because the value of Λ was increased in order to produce the rightward shift. This means that the free energy Eq. (2.31) increased. We thus can also disregard lines of constant Λ that enter the plot. In short, broken symmetry states that minimize the free energy are represented by straight lines in the Kim plot that graze the border of the plot without entering it, which is precisely the essence of the method developed by Kim [14].

We are now in a position to construct a phase diagram for $l = 7$ symmetry breaking. Restricting ourselves to constant energy surfaces in the form of straight lines that touch the Kim plot at one point, there is only one physical parameter that can be varied, namely the angle θ of the lines. Start from the dashed black line that passes through the blue point corresponding to tetrahedral symmetry (with $\theta = -.01$). It is evident that tetrahedral symmetry has a large stability range, since lines passing through the blue point can be drawn over a range of angles. Continue to increase θ. When the angle reaches 0.01, the constant Λ line (red dashed line) grazes the Kim plot at a point where a line of sixfold symmetry states just touches the border of the Kim plot (see Fig. 8). Continuing on in this fashion, one finds that the system passes through states with fivefold symmetry, again sixfold symmetry, and then sevenfold symmetry. The stability range is small for six- and fivefold symmetries, while the sevenfold symmetry state has a larger stability interval. We observe that prominent asperities of the Kim plot correspond to states with large stability intervals.[4]

---

[4]As an additional validation of the Kim method, we directly verified the thermodynamic stability of all solutions identified through that approach and listed above with the use of the Hessian matrix [5,10].
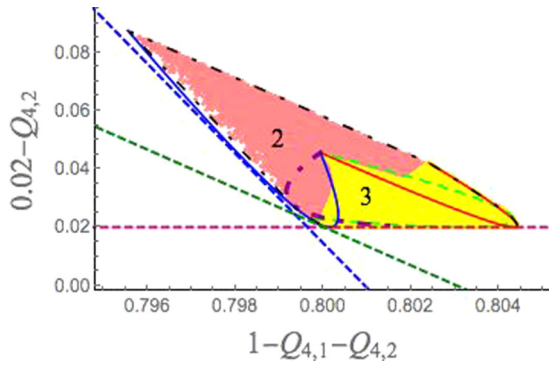
FIG. 10. Kim construction for the shifted Kim plot with newly defined quartic invariants. The symmetries are sevenfold (blue dashed line grazing the left boundary of the region), threefold (green dashed line grazing the lower left-hand corner), and multiple (horizontal red dashed line).

FIG. 11. Example of the outcome of an "ordering" transition for the Kim plot shown in Fig. 10 in which the only quartic invariant is proportional to $Q_{4,2}$ and there is a continuous degeneracy. The degeneracy is signaled by the extended contact between to the red dashed line and boundary of the Kim plot. Other possible symmetries in this case are two-, three-, and fivefold.

A phase diagram for $l = 7$ can be obtained by the following steps: (i) construct the Kim plot; (ii) draw a family of lines that graze the Kim plot; and (iii) plot the symmetry of the point on the boundary of the Kim plot as a function of the angle of the straight lines. The final step is to determine the relation between the angle θ and the thermodynamic parameters that enter the Landau variational free energy. If we assume that a is positive and that b and c are negative, then this last step excludes lines that graze the Kim plot along the solid blue border of the Kim plot and along the horizontal border that runs along the top of the plot at $Q_{4,2} = 0$. A phase plot is shown in Fig. 9. While the reduced transition temperature for states with different symmetry is the same, that does not mean that there can be no transitions between states of different symmetry when the physical temperature is varied because the system parameter θ could depend on the physical temperature.

Next, assume that a is negative while b and c are positive, with a small enough so the overall sign of the quartic term remains positive. While this is (probably) an unphysical range, this case provides useful insights into the Kim construction. Figure 10 shows an example of the Kim plot and construction for that case. The net effect is an overall rigid-body translation and rotation of the Kim plot. The Kim construction now is focused on the vertex of the Kim volume that previously was inaccessible in Fig. 7. As noted in the caption to Fig. 10, there are now three regimes.[5] The ordering has a sevenfold axis in the regime associated with the dashed blue line along the left-hand side of the volume and a threefold axis in the regime indicated by the dashed green line at its lower left-hand corner. The fourth regime, indicated by the horizontal red line, allows for a variety of symmetries as a result of the degeneracy of state with respect to the local invariant $Q_{4,1}$. This is because of the structure of the mediated invariant $Q_{4,2}$, which is now the sole quartic invariant in the free energy. In this case, the ordered state allows for a continuous, degenerate set of $\{\psi_k\}$ angles. The ordering possibilities include a twofold symmetry axis, a threefold axis, a fivefold axis, a sixfold axis, sevenfold symmetry, and tetrahedral ordering. Additionally, the ordering
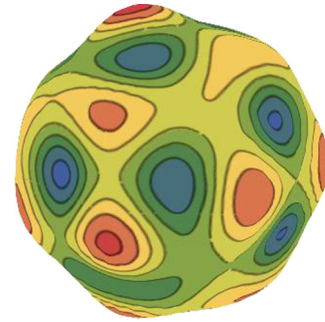
may have no discernible symmetry at all; an example is shown in Fig. 11. As shown in the Supplemental Material [16], the degeneracy arises from the structure of the quadratic invariant $Q_{4,2}$. One might expect a physical realization of such a system to have the character of an *orientational glass*. A phase plot for negative a as a function of θ is shown in Fig. 12. Figure 13 shows realizations of the density associated with some of the other $l = 7$ symmetric structures.

The numerical effort involved in the Kim construction appears to be minimal as compared to a brute-force minimization of the Landau functional in a 15-dimensional space. This is indeed the case if one accurately knows the Kim plot. However, the boundary of the Kim plot of Fig. 7 was obtained by random sampling and along part of the dash-dotted line of Fig. 7 the boundary is quite sparse. This is because the Kim plot is in this case actually the projection of a five-dimensional volume onto a two-dimensional plane. Consequently, random sampling can be expected to generate a far higher fraction of points in the interior of the volume than near its surface. This problem will only become worse for larger values of l. Because the precise location of the boundary of the Kim plot is crucial for predicting the possible symmetries of free-energy minima, we developed a convenient method to precisely trace out the boundary of the Kim plot for any symmetry of interest, which is described in Appendix C.
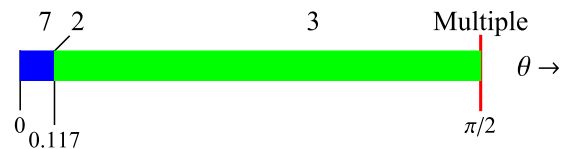

FIG. 12. Schematic phase diagram for $l = 7$ for the case that the system parameter a is negative while b and c are positive. For increasing θ and negative t_7, the system passes from a state with a sevenfold axis (blue) to a state with a threefold axis (green). As indicated in the figure, there is also a very narrow window between the three- and sevenfold states in which the minimum free energy possesses twofold symmetry. If $\theta = \pi/2$, then a continuous degeneracy arises, which allows for a multiplicity of minimum free-energy states.

___

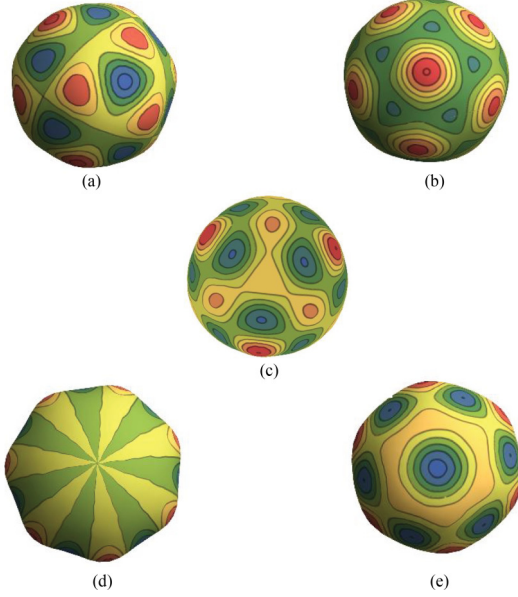[5]Actually, there is a fourth regime; see Fig. 12.

FIG. 13. Symmetric states encountered for the Kim plot $l = 7$ (a) tetrahedral, (b) fivefold, (c) threefold, (d) sevenfold, and (e) sixfold.

2. $l = 6$

Our next example is the Kim construction for $l = 6$. First, consider the case that only the local quartic invariant is kept. To find the transition temperature t_c, we then only need to maximize the ratio $Q_3(\{\psi_i\})^2/Q_4(\{\psi_i\})$. It is instructive to do this by adapting the Kim method. Construct a two-dimensional invariant space with $Q_3(\{\psi_i\})^2$ and $Q_4(\{\psi_i\})$ as the coordinate axes and construct a Kim plot by random sampling of the two invariants over the allowed set of orientations $\{\psi_i\}$. As shown in Fig. 14, the resulting Kim plot has three sharp corners.

The Kim construction that finds t_c involves drawing straight lines starting at the origin in the Q_4-Q_3^2 plane with various slopes, corresponding to fixed values of $t_6 = Q_3(\{\psi_i\})^2/Q_4(\{\psi_i\})$ for that orientation in the 13-dimensional configuration space. The highest transition temperature corresponds to the line with the highest slope that just grazes the Kim plot at its tip, which has icosahedral symmetry, so the Kim construction reproduces the results of SRN. For lower values of t_6, we need to draw lines of constant free energy $\mathcal{F}_{\min}$ in the Kim plot. Such contours are constructed in Appendix D, with an example shown in Fig. 38.

Next, include the trivial and $j = 2$ mediated invariants. Using the notation of the previous section, the full $l = 6$ Landau free energy can be written as

$$\mathcal{F}_6 = \frac{t_6}{2}A^2 + \frac{u}{3}A^3 Q_3 + \frac{v}{4}A^4\{[(Q_{4,1} + 0.95Q_{4,2}) - X_0]\cos\theta$$
$$+ (Q_{4,2} - Y_0)\sin\theta\} \tag{2.34}$$

and the transition temperature that needs to be maximized is

$$t_6 = (u^2/9u)$$

$$\times \frac{Q_3^2}{\{[(Q_{4,1} + 0.95Q_{4,2}) - X_0]\cos\theta + (Q_{4,2} - Y_0)\sin\theta\}} \tag{2.35}$$
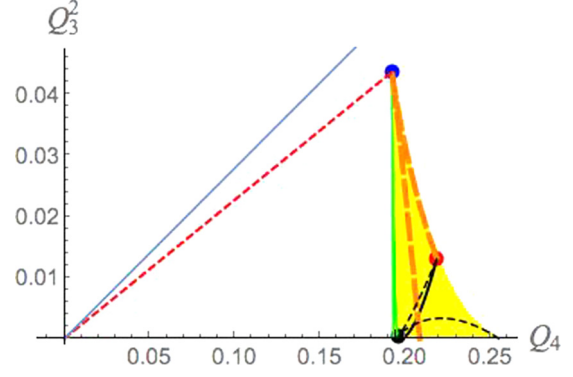

FIG. 14. Kim plot for $l = 6$ with only the local invariant. The curves in the Kim volume correspond to symmetries as follows: solid black curve, a single fourfold symmetry axis; thick, dashed orange curve, single fivefold axis; dashed black curve, a single sixfold axis; and green curve along the left-hand border of the Kim volume, tetrahedral symmetry. The apex of the plot has icosahedral symmetry, as indicated by the blue point. The red point on the right-hand boundary corresponds to D_∞ symmetry, and the black point on the lower left-hand corner corresponds to octahedral symmetry. The slope of the dashed red curve indicates the highest possible ratio of $Q_3(\{\psi_i\})^2/Q_4(\{\psi_i\})$ and hence the highest value for t_6 at the transition. The black line, which misses the Kim volume, represents a higher value of the ratio that is not physically realized.

(where we did not explicitly display the dependence on the angle variables ψ_i).

The Kim plot is now a three-dimensional volume with a tentlike, concave surface spanned between four sharp corners. Redefine the coordinate axes as $X = Q_{4,1} + 0.95Q_{4,2}$, $Y = Q_{4,2}$, and $Z = Q_3^2$ (the small numerical shift in the definition of the X coordinate is for visual convenience.) Figures 15 and 16 show different perspectives of the three-dimensional Kim plot in the space spanned by these three axes. The thick orange curve is a ridge with fivefold symmetry; the green curve on the right-hand side of the plot corresponds to tetrahedral symmetry; the blue dot, on the upper boundary of the plot,
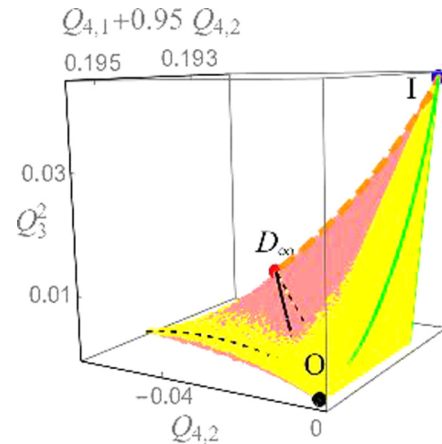

FIG. 15. The Kim plot for $l = 6$ including all quartic invariants. The labeling I, O, and D_∞ identify points corresponding to icosahedral, octahedral, and D_∞ symmetry. For a description of the curves, see the accompanying text.
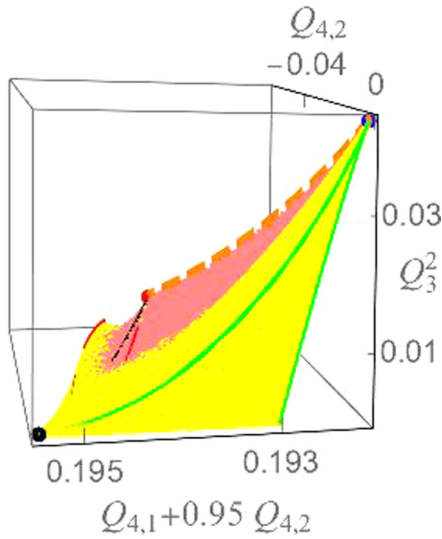
FIG. 16. Second perspective of the $l = 6$ Kim plot.

FIG. 17. The intersection of a constant free-energy surface with the icosahedral symmetry point in the $l = 6$ Kim plot.

corresponds to icosahedral symmetry; the black dot at the lower left-hand corner of the plot corresponds to octahedral symmetry; and the embedded purple dot at the lower end of the orange curve corresponds to D_∞ (full rotational symmetry and mirror reflection about an axis). The solid black curve corresponds to a fourfold symmetry axis and the dashed black curve to sixfold symmetry. A second perspective of the Kim plot is shown in Fig. 15. The invariant $Q_{4,2}$ is zero in the facing surface. The green tetrahedral symmetry curve has two branches that meet each other and the fivefold symmetry curve at the icosahedral symmetry point. The upper branch ends at the lower left-hand corner of the plot, also a sharp point, at the black dot corresponding to the octahedral symmetry point noted earlier.

Following the same steps as before, we first use the Kim method to locate the transition temperature t_c. This requires maximizing

$$t_6 = \frac{Q_3^2}{\{[(Q_{4,1} + 0.95Q_{4,2}) - X_0]\cos\theta + (Q_{4,2} - Y_0)\sin\theta\}}. \tag{2.36}$$

Surfaces of constant t_6 are planes in the three-dimensional invariant space. The surface with largest t_6 value that just grazes the "Kim volume" determines the symmetry of the first broken symmetry state when t_6 is reduced. For temperatures below t_c, we need to construct surface of constant free energy. As can be expected from the case of only local invariants, these surfaces are not flat planes. Figure 17 shows an example of a constant free-energy surface passing through the point of icosahedral symmetry. The minimum free-energy state *always* has icosahedral symmetry for the physical case that the coefficient a of the local quartic invariant is positive while the coefficients b and c of the nonlocal invariants are negative. We show in the Supplemental Material [16] that if the local quartic invariant has a negative coefficient and the nonlocal quartic invariants have positive coefficients, then octahedral, sixfold, and D_∞ symmetries can be realized, together with
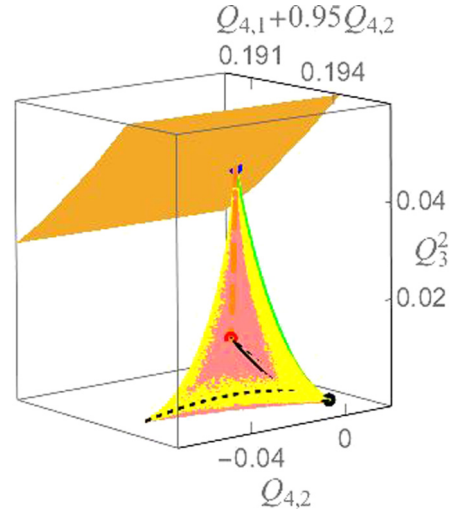
icosahedral symmetry, in agreement with the findings of Jarić [12]. A phase plot is shown in Fig. 18.

III. ORIENTATIONAL ORDERING AND THE KIM CONSTRUCTION FOR $l = 15 + 16$

With the experience gained for $l = 6$ and $l = 7$, we now apply the Kim construction to the $l = 15$ and $l = 16$ sectors that are the focus of our physical interest. We will restrict ourselves to a variational free energy with only local invariants; even with this simplification, there still are six local cubic and quartic invariants in the combined $l = 15 + 16$ sector. While we know of no simple method that would allow us to carry out complete Kim constructions in a six-dimensional space, it is possible—as we will demonstrate—to combine Kim plots for restricted versions of the variational free energy with numerical minimization to arrive at a reasonably complete analysis. We start by examining the $l = 15$ and $l = 16$ sectors separately.

A. The $l = 15$ sector

As for $l = 7$, the $l = 15$ ordering transition is continuous because of the absence of a cubic invariant. If only the single local quartic invariant is included, then the state with minimum free energy corresponds to the minimum of the ratio of quartic invariant Q_4 and the square of the quadratic
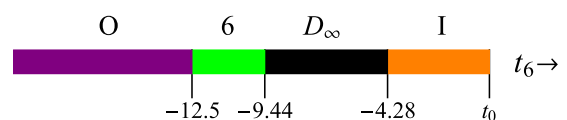

FIG. 18. Schematic phase diagram for $l = 6$ for the case that the system parameter a is negative while b and c are positive. The octahedral portion continues to arbitrarily large and negative t_6. The value of t_0 is 0.0017.

TABLE I. Ordered list of minimum values of the invariant combination, $\mathcal{R}$ as defined in (3.1), by imposed symmetry. Note that the magnitude for C_5 is the same as the magnitude for no imposed symmetry.

Symmetry	Magnitude of the invariant $\mathcal{R}$
All	0.208797
C_5	0.208797
C_3	0.208809
C_2	0.208857
C_7	0.208904
C_4	0.209495
T	0.210448
C_6	0.21052
I	0.210534
C_{11}	0.21121
C_{12}	0.211582
C_{10}	0.212131
C_{13}	0.213575
C_9	0.214088
C_8	0.217175
C_{14}	0.21796
O	0.220681
C_{15}	0.227049
C_∞	0.261008

invariant Q_2:

$$\mathcal{R} \equiv \frac{\langle \rho_{15}^4 \rangle}{\langle \rho_{15}^2 \rangle^2} = Q_4. \quad (3.1)$$

Numerical values of $\mathcal{R}$ are displayed in Table I. In the table, T refers to tetrahedral symmetry, O to octahedral symmetry, and I to icosahedral symmetry. The fact that odd-l spherical harmonics are odd under reflection precludes D_n symmetry. The top entry, labeled "All," records the result of an unconstrained search for the minimum quartic invariant. The entry labeled "C_5" gives the value of $\mathcal{R}$ for a state with a fivefold symmetry axis. The two values are identical. Comparison with the results of numerical minimization using the method of Refs. [5,10] confirms that the global minimum in the $l = 15$ sector has C_5 symmetry.

The Hessian matrix—constructed by taking the second derivative of the quartic magnitude with respect to the $2l + 1 = 31$ degrees of freedom of the density [5,10]—allows us to assess the stability of the various symmetry states. This matrix has three zero eigenvalues corresponding to the generators of global rotations in three dimensions. If all other eigenvalues are positive, then the symmetry state is locally stable with respect to infinitesimal distortions of the density. If any of the other eigenvalues is negative, then the quartic term can be reduced by introducing an additional density that distorts the symmetry. In this way, we find that the C_5 state is stable. The C_3 state also is stable and corresponds to a metastable free-energy minimum. None of the other symmetries were found to be stable. The table highlights an important point. The difference between the values of $\mathcal{R}$ for the C_5 and C_3 states appears only in the *fifth* decimal: The two states are practically degenerate. The other symmetry states listed in the table are all unstable and have comparable values of $\mathcal{R}$. The
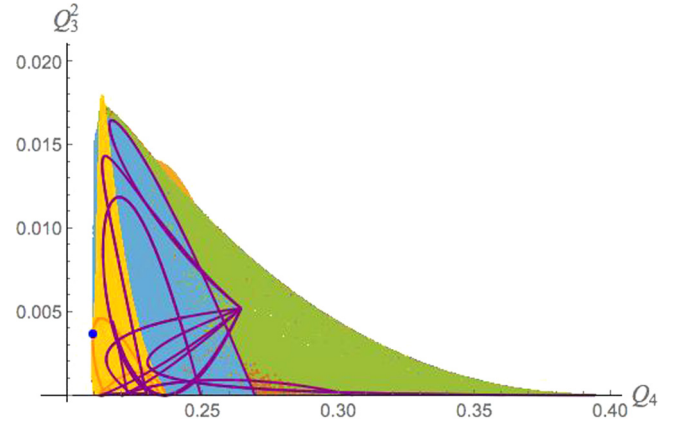

FIG. 19. The Kim plot for $l = 16$ with only local invariants. The symmetries corresponding to the prominent colored regions are sevenfold (green region on the far right, also protruding on the upper left-hand side), tetrahedral (orange region on the left), and eightfold (blue region just to the right of the tetrahedral region). The various dark purple curves correspond to symmetries ranging from nine- to 16-fold. Those curves meet at a point in the interior of the Kim region corresponding to D_∞ symmetry. The orange curve in the lower left-hand portion of the Kim region corresponds to octahedral symmetry. The blue dot on the leftmost boundary is the point of icosahedral symmetry.

free-energy landscape of the $l = 15$ sector is apparently quite flat with only a few shallow minima.

B. The $l = 16$ sector

For $l = 16$, we follow the same steps as for $l = 6$ with local invariants. There is a single cubic invariant, Q_3—so the ordering transition must be first order—and a single quartic invariant, Q_4. The state that appears at the point where the symmetry of the uniform state is broken corresponds to a maximum the ratio Q_3^2/Q_4. Figure 19 shows the corresponding Kim volume.

Just as for $l = 6$, the Kim plot has a roughly triangular outline with a protruding tip, but here there is a crucial difference. For $l = 6$, a unique state with icosahedral symmetry was located at the tip, with the result that only states with icosahedral symmetry emerged from the Kim construction. For $l = 16$, this icosahedral state is missing from the tip. By contrast, the tip has tetrahedral symmetry everywhere for $l = 16$.[6] An enlarged version of the tip region is shown in Fig. 20. The tetrahedral point on the border of the Kim plot that maximizes Q_3^2/Q_4 is indicated by a red dot.

While icosahedral symmetry has been demoted from the prominent position it had for $l = 6$, it has not completely disappeared. There is a point with icosahedral symmetry on the boundary line of the Kim plot located at the tip of a small asperity in the lower left-hand side of the plot (see Fig. 21).

We can now carry out the Kim construction in the case of $l = 16$. The result is shown in Fig. 22.

---

[6]That the initial ordering in the case $l = 16$ should be tetrahedral was noted by Matthews [11].
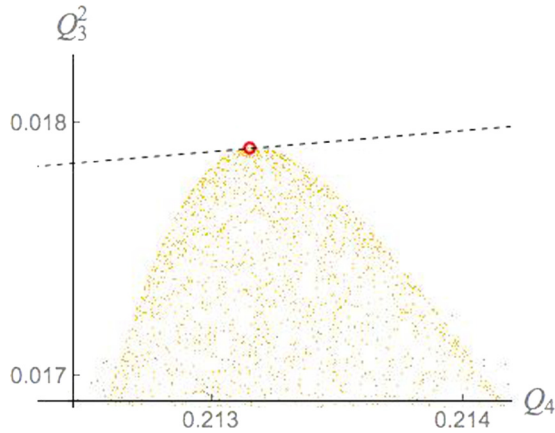
FIG. 20. The Kim plot in the vicinity of the tip at the top of the plot. The open red dot corresponds to the point on the border of the Kim plot that maximizes Q_3^2/Q_4, as indicated by the line passing through it. The stippled region has tetrahedral symmetry.

If the coefficient t_{16} of the quadratic invariant is reduced starting in the isotropic state, then the first nonuniform state that appears has tetrahedral symmetry. It corresponds to the red dot in Fig. 20. The value of the cubic invariant at the transition point (see Fig. 20) is significant, so it is a robust first-order transition. As the temperature is lowered, the tetrahedral state transits to a state with threefold symmetry, then to a state with sevenfold symmetry, then again to a state with threefold symmetry, and then finally to a state with icosahedral symmetry. The phase plot is shown in Fig. 23.

It is useful to complement the Kim construction for $l = 16$ with direct free-energy minimization to obtain explicit density profiles. Figure 24 shows examples that exhibit some of the symmetries obtained by numerical minimization of the local free energy for appropriate values of the coefficients of the quadratic, cubic, and quartic invariants. We set here $u = v = 1$, where u is the cubic coefficient and v is the quartic coefficient; see, for example, Eq. (3.8). In the earlier studies based on numerical free-energy minimization [5,10], we missed the $l = 16$ icosahedral state in the phase plot, which will play a key role in the discussion immediately below. The utility of
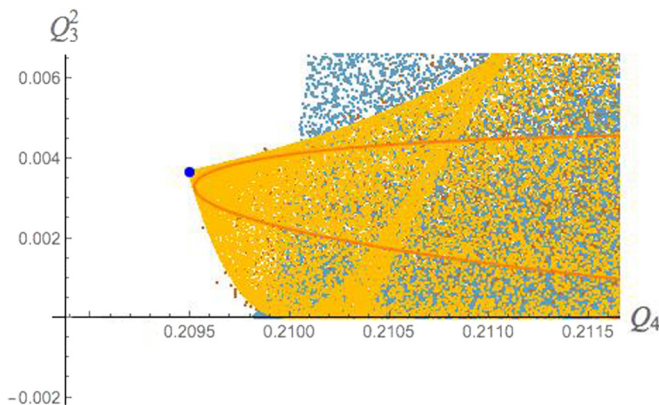

FIG. 21. The Kim plot in the vicinity of the icosahedral asperity. The orange parabolic curve corresponds to octahedral symmetry, which does not quite extend to the icosahedral point.
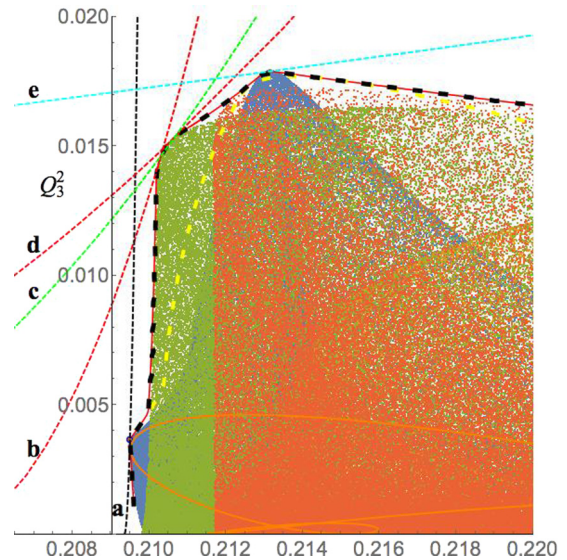

FIG. 22. Kim plot and construction for $l = 16$ with local invariants. Curves outlining the boundary of the Kim plot are colored according to symmetry: fivefold (dashed light yellow curve), threefold (solid red curve), and twofold (dashed black curve). The dashed constant free-energy curves of the Kim construction that graze the surface at a certain point on the boundary of the Kim plot are colored in correspondence to the symmetry of the point: In decreasing order of slope value, the labeled constant free-energy curves grazing the surface of the Kim volume at various symmetry points are (a) icosahedral symmetry (nearly vertical dashed blue curve); (b) threefold symmetry (dashed red curve); (c) sevenfold symmetry (dashed green curve); (d) threefold symmetry again (dashed red curve); and (e) tetrahedral symmetry (dashed light blue curve).

the Kim plot for the numerical minimization is evident: The symmetries that will be realized by the Kim construction are obvious by inspection.

C. The $l = 15 + 16$ sector for fixed mixing ratio

Now we turn to the Kim construction in the enlarged $l = 15 + 16$ space. As noted, the number of local invariants is significant. There are separate quadratic and quartic invariants for $l = 15$ and for $l = 16$. Next there is the cubic invariant for $l = 16$ as well as the mixed cubic invariant $\langle \rho_{16} \rho_{15}^2 \rangle$, and finally the mixed quartic invariant $\langle \rho_{15}^2 \rho_{16}^2 \rangle$. To obtain insight, we used two different strategies. The first, discussed here, is to fix the relative contribution of $l = 15$ and $l = 16$. Define

$$\rho_{15} = \cos \eta \, A \, q_{15}\big(\psi_i^{(15)}\big), \tag{3.2}$$

$$\rho_{16} = \sin \eta \, A \, q_{16}\big(\psi_i^{(16)}\big), \tag{3.3}$$
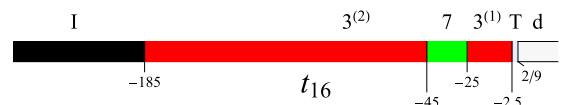

FIG. 23. Sequence of states produced by the Kim construction for $l = 16$ as a function of the coefficient t_{16} of the quadratic invariant. T, tetrahedral; $3^{(1,2)}$, two states with a three-fold axis; 7, sevenfold axis; I, icosahedral; and d, disordered. The phase diagram was calculated for coefficients $u = v = 1$; see Eq. (3.8).
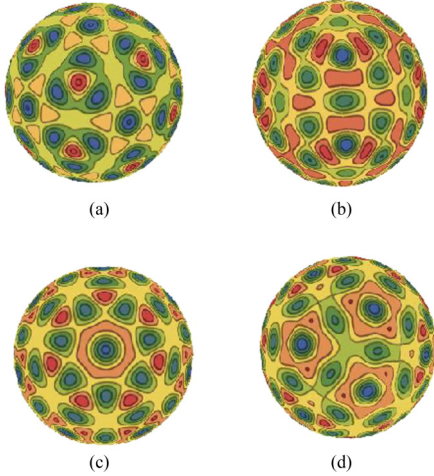
FIG. 24. The various symmetries that are possible for a purely local $l = 16$ free energy as obtained from a numerical minimization of a variational free energy with one quadratic invariant, one cubic invariant, and one quartic invariant. The symmetries are (a) icosahedral, (b) tetrahedral, viewed along a twofold axis, (c) sevenfold, and (d) threefold. The last two symmetries are those of an antiprism.

where $0 \leqslant \eta \leqslant \pi/2$ is a "mixing angle" and where and $\psi_i^{(15)}$ and $\psi_i^{(16)}$ refer to the set of $2l$ internal angular variables that determine the precise forms of the two densities. The two quadratic invariants are

$$\langle \rho_{15}^2 \rangle = A^2 (\cos \eta)^2, \tag{3.4}$$

$$\langle \rho_{16}^2 \rangle = A^2 (\sin \eta)^2, \tag{3.5}$$

where for any function $f(\theta, \phi)$,

$$\langle f \rangle = \int f(\theta, \phi) \, d\Omega. \tag{3.6}$$

Since $(\tan \eta)^2 = \rho_{16}^2 / \rho_{15}^2$, the mixing angle is an invariant in its own right. We will include it in the form of the relative participation $(\sin \eta)^2 = f_{16}$ of the $l = 16$ density to the total density. If one fixes f_{16}, then one is effectively down to three invariants, a situation that can be managed by the methods described earlier. Figure 25 shows the Kim region for the case that f_{16} is fixed at 0.05. This Kim plot now has *two* vertical protrusions: the left protrusion has tetrahedral symmetry and the right protrusion has 13-fold symmetry. Surprisingly, the icosahedral point has "slid upward" to a location close to the tip of the protrusion. Now, the tetrahedral state has to compete with the icosahedral state. Figure 26 shows the portion of the plot in Fig. 25 that contains the promoted icosahedral point (shown solid and in blue) and also the point corresponding to the largest transition temperature in the Kim construction (the open green point). In an ensemble in which relative contributions from $l = 15$ and $l = 16$ are set at 0.95 and 0.05 respectively, the initial transition is to tetrahedral symmetry. As the quadratic coefficients are reduced, icosahedral symmetry takes over. The salient point is that the Kim plot of a dominant $l = 15$ state with a small admixture of $l = 16$ is qualitatively different from that of the pure $l = 15$ Kim plot. Icosahedral symmetry appears to be here intrinsically
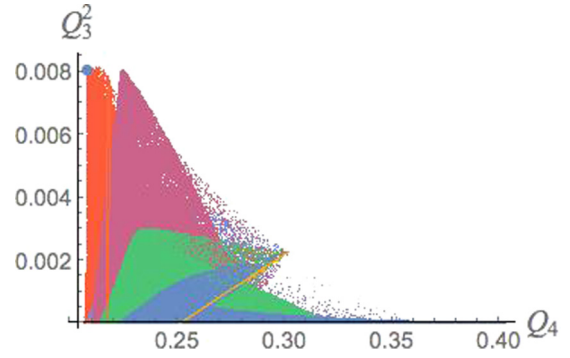

FIG. 25. The $l = 15$ and 16 Kim plot when $f_{16} = 0.05$. The blue dot on the upper left boundary of the plot is the point of icosahedral symmetry. The red portion on the left of the Kim volume on whose boundary the dot sits corresponds to tetrahedral symmetry. The purple protrusion to its right is a region of 13-fold symmetry. The prominent green region in the lower left-hand portion of the plot corresponds to 10-fold symmetry.

associated with a mixed $l = 15 + 16$ state while it is largely unstable for pure $l = 15$ and $l = 16$ order parameter states.

It again is useful to combine the Kim construction with the outcome of direct numerical minimization producing a representative phase diagram. We allowed η and f_{16} to vary freely, while for the variational free energy we used

$$
\begin{aligned}
F &= \frac{t_{15}}{2} \langle \rho_{15}^2 \rangle + \frac{t_{16}}{2} \langle \rho_{16}^2 \rangle + \frac{u}{2} \langle (\rho_{15} + \rho_{16})^3 \rangle + \frac{v}{4} \langle (\rho_{15} + \rho_{16})^4 \rangle \\
&= \frac{t_{15}}{2} \langle \rho_{15}^2 \rangle + \frac{t_{16}}{2} \langle \rho_{16}^2 \rangle + \frac{u}{3} \left(\langle \rho_{16}^3 \rangle + 3 \langle \rho_{16} \rho_{15}^2 \rangle \right) \\
&\quad + \frac{v}{4} \left(\langle \rho_{15}^4 \rangle + 4 \langle \rho_{15}^2 \rho_{16}^2 \rangle + \langle \rho_{16}^4 \rangle \right).
\end{aligned}
\tag{3.7}
$$

In arriving at the last line, we used the symmetry properties of $\rho_{15}(\theta, \phi)$ and $\rho_{16}(\theta, \phi)$ under reflection. Because of the orthogonality of the $l = 15$ and $l = 16$ densities, the square of the total density, $\langle \rho^2 \rangle$, is $\langle \rho_{15}^2 \rangle + \langle \rho_{16}^2 \rangle$. Next, because of the second cubic term, a nonzero $l = 15$ density necessarily entrains an $l = 16$ density but the the reverse is not true. This means that pure $l = 16$ states are possible but pure $l = 15$
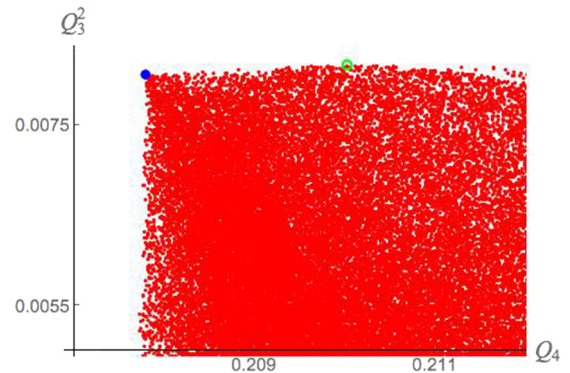

FIG. 26. Detailed portion of Fig. 25 containing the icosahedral point (blue dot on the upper left-hand corner) and the point corresponding to the highest transition temperature (open green dot at the top and to the right of the icosahedral point), along with the tetrahedral region (red stippled portion).
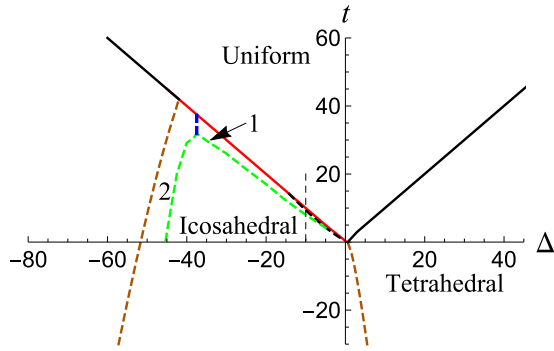
FIG. 27. Phase diagram obtained by numerically minimizing the free energy (3.8) for $u = v = 10$. The green dashed curve separates the region in which icosahedral order is a global free-energy minimum (below the curve) from the region in which it is a local, but not global, free-energy minimum. The curve corresponds to a line of first-order phase transitions. The thin vertical dashed line at $\Delta = -10$ indicates the parameter range plotted in Fig. 28. The brown dashed lines indicate stability limits of icosahedral symmetry, corresponding to spinodal lines. Finally, the blue dashed line between the green curve and the line of transitions from uniform to ordered phases separates the two regions of nonicosahedral order: tetrahedral (region 1) and nontetrahedral (region 2).

states are not. Note that this is not the most general local variational energy: The cubic and quartic contributions were expressed in terms of the total density ($\rho_{15} + \rho_{16}$) but the $l = 15$ and $l = 16$ quadratic invariants have separate prefactors t_{15} and t_{16} for the corresponding density.

The result of numerical free-energy minimization for $u = v = 10$ is shown in Fig. 27.[7] The t and Δ axes are defined by the relations $t_{15} = t + \Delta$ and $t_{16} = t - \Delta$. The phase diagram has four principal regions. The top region is the uniform state. It is bordered by a wedge of solid black lines that separates it from the phases with orientational order. In the region below the wedge to the right, the order is pure $l = 16$ with tetrahedral symmetry. In the third region, labeled "icosahedral," a mixed state with icosahedral symmetry is at least locally stable but it is only the global free-energy minimum below the green dashed curve. Between the green dashed curve and the two nearly vertical solid black lines, other symmetries have lower free energy. The two dashed brown lines play the role of *spinodals* for the icosahedral state. The red line along the top of the icosahedral region marks either continuous or weakly first-order transitions from the isotropic state to a tetrahedral state that quickly transforms to an icosahedral state as the temperature is lowered further. Even when the parameter $\Delta = (t_{15} - t_{16})/2$ is as low as -50, the tiny amount of residual $l = 16$ density suffices to destabilize the C_5 minimum free-energy state of pure $l = 15$. This is consistent with our earlier observations concerning the fragility of the free-energy minimum of the pure $l = 15$ sector. Finally, the fourth region to the left of the icosahedral region has complex symmetries that are neither icosahedral nor does

it have the C_5 symmetry of pure $l = 15$, again a consequence of the near degeneracy of the $l = 15$ sector.

The numerical results can be compared with the Kim construction for fixed mixing ratio. The Kim construction predicted that the icosahedral state should be stable over a large range of parameters but that the symmetry-breaking transition of the uniform state should produce a tetrahedral state with a narrow stability interval. The utility of the Kim construction is obvious: It would be easy to miss the tetrahedral sliver in a numerical minimization while the tetrahedral state is obvious by inspection of the Kim plot. In summary, numerical minimization of the variational free energy in the enlarged $l = 15 + 16$ space of invariants confirms that the icosahedral state is globally stable over a significant parmeter range. The region of icosahedral stability is separated from the uniform region by a narrow interval of tetrahedral dominance.

Finally, how good is the assumption that f_{16} is constant? Figure 28 shows a plot of dependence of f_{16} on t for fixed $\Delta = -10$. For large and negative t, f_{16} varies only modestly so the assumption of fixed f_{16} is reasonable. However, the assumption of fixed f_{16} definitely fails near the onset of orientational ordering with f_{16} going linearly to zero at the
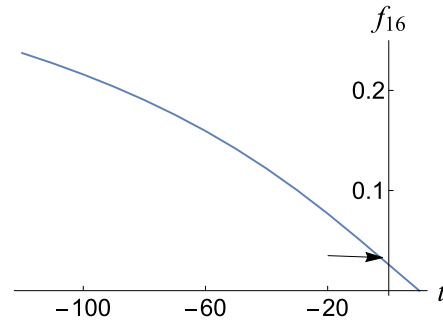

FIG. 28. The fractional participation of $l = 16$ in the total density, labeled by f_{16}, is plotted as a function of t for fixed $\Delta = -10$, along the vertical dashed line in Fig. 27 (and its extension to negative values of t). For the very rightmost values of t, the density is tetrahedral. The arrow identifies the point at which the minimum free-energy symmetry changes from tetrahedral to icosahedral. The curve hits the horizontal axis at the onset of ordering.
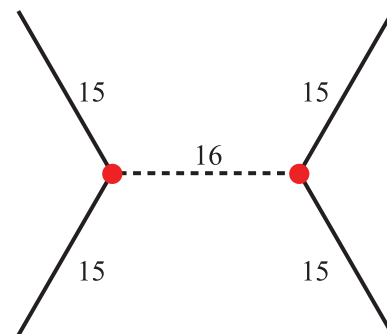

FIG. 29. Diagrammatic representation of the nonlocal quartic term generated in the $l = 15$ free energy by integrating out the $l = 16$ density. The dashed line represents the $l = 16$ propagator with a weight $1/t_{16}$ and the two red dots represent the three-point vertex with a weight u.

---

[7]This figure is an elaborated version of a phase diagram for the same system in Ref. [5].
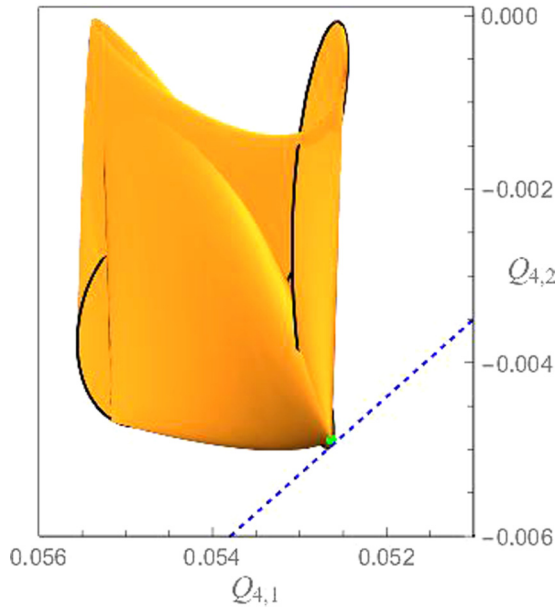
FIG. 30. The Kim plot for $l = 15$ with the $l = 16$ contribution integrated out to lowest nontrivial order. The term $Q_{4,1}$ is the local quartic term for $l = 15$ and the term $Q_{4,2}$ is the new nonlocal quartic term. Only states with tetrahedral symmetry are included, along with the state with icosahedral symmetry represented by the green dot. The black curve denotes the edge of the region with tetrahedral symmetry, which is a self-intersecting two-dimensional surface. The dashed blue line depicts a constant free-energy surface that grazes the boundary of the tetrahedral symmetry region and also the boundary of the full Kim plot. It passes close to the green icosahedral symmetry point, but it does not impinge on it, as shown in Fig. 31.

transition point. This can be understood from the form of the coupling term $u\langle\rho_{16}\rho_{15}^2\rangle$ between the $l = 15$ and $l = 16$ states. Combined with the term that is quadratic in ρ_{16}, it follows that, just below the ordering temperature, the average $\langle\rho_{16}\rangle$ is proportional to $\frac{u}{t_{16}}\langle\rho_{15}\rangle^2$. Since there is no cubic invariant in the $l = 15$ sector, it follows that $\langle\rho_{15}^2\rangle$ goes to zero linearly at the transition point so the participation ratio $\langle\rho_{16}\rangle^2/(\langle\rho_{15}\rangle^2 + \langle\rho_{16}\rangle^2)$ also goes linearly to zero. Close to the ordering transition, we need a different approach that will be discussed in the next section.

From the viewpoint of Landau theory, these results are disconcerting. While it is reasonable that $l = 15$ ordering will entrain a certain amount of $l = 16$ density as a secondary order parameter—because of the mixed cubic invariant $\langle\rho_{16}\rho_{15}^2\rangle$—it is anomalous that the mixing between primary and secondary order parameters ($l = 15$, respectively, $l = 16$) destabilizes the primary $l = 15$ order parameter (with C_5 fivefold symmetry) and that it stabilizes an icosahedral state that is either unstable or only accessible well below the ordering temperature in the single l subspaces. It would seem that canonical Landau theory, based on a dominant order parameter that transforms according to a single irreducible representation of the high-temperature symmetry group, does not produce the actual minimum free-energy state. In the next section, we will see why this conclusion has to be modified.
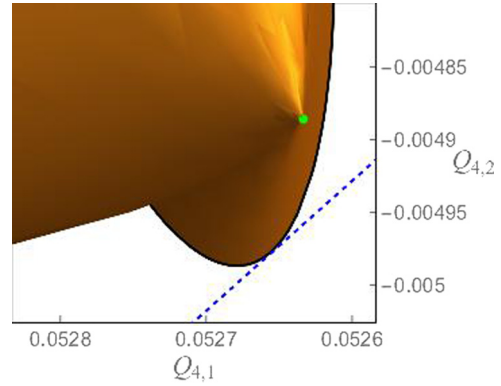

FIG. 31. The portion of the Kim plot shown in Fig. 30 containing the icosahedral point. The icosahedral point is located in the interior of the Kim plot and lies at the tip of a small conical protuberance in a third dimension. As shown in Fig. 30, the constant free-energy surface indicated by the dashed blue line grazes the surface of the tetrahedral symmetry region.

D. Diagrammatic perturbation theory and the Kim construction

In this final subsection, we use the Kim construction to investigate the competition between icosahedral and tetrahedral symmetry close to the ordering transition where f_{16} is very small. This second method is based on *perturbation theory*. It starts from the assumption that the contribution from $l = 16$ contribution is sufficiently small that the $l = 16$ density can be described by a quadratic Hamiltonian. Expanding the variational free energy to second order in $\rho_{16}(\mathbf{\Omega})$ gives

$$\Delta H_{16} \simeq \int d\mathbf{\Omega}\left(\frac{t_{16}}{2}\rho_{16}(\mathbf{\Omega})^2 + u\rho_{16}(\mathbf{\Omega})\rho_{15}(\mathbf{\Omega})^2\right) \quad (3.8)$$

with t_{16} positive. The next step is to integrate out $\rho_{16}(\mathbf{\Omega})$ to arrive at a renormalized variational free energy for $\rho_{15}(\mathbf{\Omega})$. The mathematical steps of integrating out the $l = 16$ component are very similar to the steps that are taken if one integrates out shape fluctuations (see the Supplemental Material [16]). Just as in that case, the integration generates a negative, nonlocal
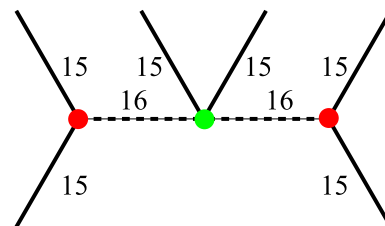

FIG. 32. Diagrammatic representation of a sixth-order nonlocal contribution to the $l = 15$ variational energy generated by integrating out the $l = 16$ contributions perturbatively to second order in $1/t_{16}$. The red dots on the two sides represent the three-point vertex with weight u and the green dot at the center a four-point vertex with weight v.

quartic contribution to the $l = 15$ variational free energy:

$$-\frac{u^2}{2t_{16}} \sum_{m=-16}^{16} \int d\boldsymbol{\Omega} \int d\boldsymbol{\Omega}' \rho_{15}(\boldsymbol{\Omega})^2 Y_{16}^m(\boldsymbol{\Omega}) Y_{16}^m(\boldsymbol{\Omega}')^* \rho_{15}(\boldsymbol{\Omega}')^2.$$

$$(3.9)$$

Using the notation introduced in Sec. II, this term can be represented by the graph shown in Fig. 29. Two three-point vertices are connected by an $l = 16$ "propagator." By connecting two of the external lines in the graph, a fluctuation correction to the quadratic term of the $l = 15$ variational energy could be generated but, in the spirit of confining ourselves to a mean-field model, we only will include tree diagram contributions in this section. So, even though we started from a local variational free energy, the step of integrating out the $l = 16$ component generates nonlocal invariants.[8]

Next, construct a two-dimensional Kim plot with the normalized local invariant and the new nonlocal quartic invariant as axes (see Figs. 30 and 31). Only states with tetrahedral symmetry are shown plus a single point with icosahedral symmetry. The tetrahedral area is folded on itself.[9] As the 31 expansion coefficients of the $l = 15$ spherical harmonics are varied over the range of allowed values, the same pair of values for the invariants $Q_{4,1}$ and $Q_{4,2}$ can be associated with different sets of expansion coefficients, which leads to fold lines. The external edges of the tetrahedral surface are indicated by a black curve. The position of the icosahedral point close to the outer edge suggests that a Kim construction could be performed that would reproduce the transition from a tetrahedral to an icosahedral state, but that is not the case. Figure 31, an enlarged version of the plot near the icosahedral point, shows why: The icosahedral point is definitely located in the *interior* of the Kim plot, which means that in actuality the icosahedral state should not show up.

Because the icosahedral point is very close to the boundary, it makes sense to include higher order terms in perturbation theory. We restart from a Hamiltonian for the $l = 16$ degrees of freedom that now includes both "three-point" and "four-point" interaction terms between $l = 16$ and $l = 15$:

$$\Delta H_{16} \simeq \int d\boldsymbol{\Omega} \left(\frac{t_{16}}{2} \rho_{16}(\boldsymbol{\Omega})^2 + u\rho_{16}(\boldsymbol{\Omega})\rho_{15}(\boldsymbol{\Omega})^2 \right.$$

$$\left. + 4v\rho_{15}(\boldsymbol{\Omega})^2\rho_{16}(\boldsymbol{\Omega})^2 \right).$$

$$(3.10)$$

Integrating out the $l = 16$ density using perturbation theory generates a sixth-order, positive, nonlocal invariant contribution to the $l = 15$ variational free energy with prefactor $u^2 v/2t_{16}^2$. It is represented by the diagram shown in Fig. 32. We will denote this new invariant by Q_6. We now can construct a three-dimensional Kim plot with the two earlier
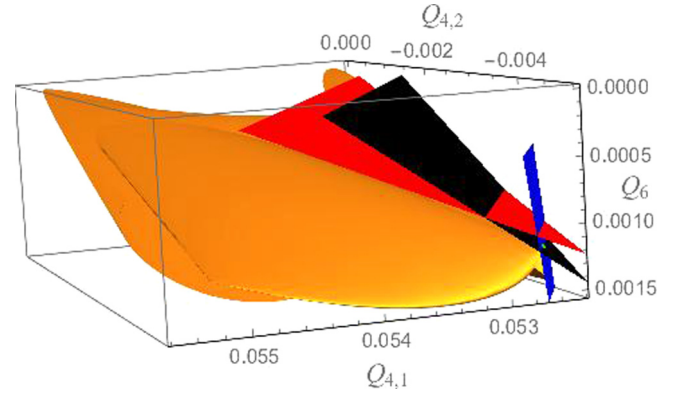

FIG. 33. The Kim plot in the three-dimensional space spanned by the two quartic terms and the sixth-order term, along with constant free-energy surfaces that grazes the Kim region at the point corresponding to icosahedral symmetry (steepest blue and less steep black surfaces) and a constant free-energy surface that grazes the plot along the tetrahedral surface (least steep red surface).

quartic invariants plus the new sixth-order invariant as coordinate axes. The icosahedral point now does lie on the boundary of the Kim plot and, as shown, it is accessible as a free-energy minimum.[10] In Fig. 33, the coefficients of the two quartic terms were arbitrarily set equal to each other, so the results shown in that figure must be viewed as qualitative. For sufficiently large negative coefficients t_{15}, the constant free-energy surface, which is nearly perpendicular to the Q_6 plane, grazes the boundary of the Kim plot along the edge of the tetrahedral symmetry surface. For sufficiently large negative coefficient t_{15} the constant free-energy surface grazes the subspace of allowed invariants through the point of icosahedral symmetry. However, as that coefficient grows in absolute value, the constant free-energy surface once again grazes the Kim plot along a point of tetrahedral symmetry. Figure 34 illustrates the sequence of states when the free energy is of the form

$$\mathcal{F}\frac{t_{15}}{2}Q_2 + \frac{v}{4}(Q_{4,1} + Q_{4,2}) + \frac{w}{6}Q_6 \qquad (3.11)$$

with $v = w = 1$.

This phase plot can be compared with that of Fig. 27 for the case that the mixing ratio between the $l = 16$ to $l = 15$ states is held fixed. In both cases, the initial symmetry-breaking transition of the uniform state leads to a state with tetrahedral symmetry. A stable icosahedral state appears as the reduced temperature is lowered further. In both cases, an $l = 16$ component is essential for the stability of the icosahedral state. The key difference is that now the phase plot formally is obtained inside the $l = 15$ sector with the $l = 16$ components absorbed by the introduction of nonlocal invariants mediated by an $l = 16$ excitation.

---

[8]For a more extended discussion of the use of perturbation theory to generate terms in the free energy, see the supporting information for Lavrentovich *et al.* [19].

[9]A MATHEMATICA.cdf document allowing for rotation of this surface can be accessed in Ref. [20].

---

[10]For the construction of a constant energy surface for a free energy with quadratic, quartic, and sixth-order terms, see the Supplemental Material [16].
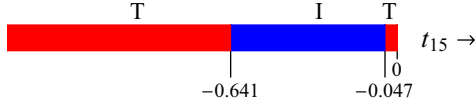
FIG. 34. Sequence of states produced by the Kim construction for $l = 15$ as a function of the coefficient t_{15} of the quadratic invariant including nonlocal invariants that are mediated by $l = 16$. T, tetrahedral; I, icosahedral. The phase plot was calculated for coefficients $v = w = 1$ in the free energy (3.11). The tetrahedral symmetry regime continues to $|t_{15}|$ well in excess of 100.

IV. CONCLUSIONS

In the introduction, we posed the question whether an order-parameter theory can be constructed for the direct transition from an isotropic state to an icosahedral state if the primary order parameter is an $l = 15$ or an $l = 16$ icosahedral spherical harmonic. We have addressed this question using the Kim construction method that allows one to obtain the general structure of a phase diagrams without having to take recourse to numerical minimization of a variational free energy for certain specific values of the physical system parameters. We found that the answer to the question is *no* if the variational free energy is constructed from the local invariants of the $l = 15$ or of the $l = 16$ sectors. In the $l = 15$ sector, the icosahedral state with local invariants was found to be completely unstable. In the $l = 16$ sector, a stable icosahedral state did appear, but only well below the orientational ordering transition. On the other hand, in the enlarged $l = 15 + 16$ space stable icosahedral states are present over a large range of system parameters—not directly abutting the isotropic state, but quite close to it—at least for fixed mixing ratio, confirming earlier numerical results [5,10]. A slice of states with tetrahedral symmetry interposes between the isotropic and icosahedral states. In the Kim construction method, the competition between the icosahedral and tetrahedral states is very clear: The Kim plot of mixed $l = 15 + 16$ states has an asperity with icosahedral symmetry that competes with a rounded peak with tetrahedral symmetry, itself a characteristic of the $l = 16$ Kim plot.

These results appear to be in glaring contradiction with the basic tenet of Landau theory that continuous phase transitions can be described by an order parameter that transforms according to a single irreducible representation of the symmetry group of the high-temperature isotropic phase. This contradiction disappeared when nonlocal invariants were included in the variational free energy: There is a stable icosahedral state in the $l = 15$ sector. By combining the Kim method with a diagrammatic perturbation expansion, we showed that the required nonlocal invariants of the $l = 15$ sector appear when a purely local free-energy functional is confined to the $l = 15$ sector by integrating out the adjacent $l = 16$ components. Because the local variational free energy in the $l = 15$ sector is quasidegenerate, the minimum free-energy state is very sensitive to the presence of even weak nonlocal $l = 15$ invariants. The nonlocal invariants necessary for the stabilization of the icosahedral state are mediated by $l = 16$.

More generally, if one starts from a variational free-energy expression with only local invariants of the density, and if the coefficient t_{l^*} of the quadratic invariant of one of the

irreducible representations is significantly lower than that of the other irreducible representations then, at the point where t_{l^*} is close to zero, the other irreducible representations can be integrated out diagrammatically, keeping such terms only to quadratic order. This procedure generates nonlocal invariants up to the maximum number permitted by the Molien polynomial.

The great advantage of the Kim geometrical method over brute-force numerical minimization is that it replaces a hit-and-miss choice of specific parameters by global geometrical analysis. The Kim construction method has already been known for decades but it is the availability of modern visualization methods that makes it such a useful tool for the study of ordering transitions in the present case. The Kim method does become cumbersome—and less revealing—if one is forced to carry out the geometrical constructions in an invariant space with more than three dimensions. Because of the proliferation of invariants for larger l, this would seem to be a serious objection because, as we have just shown, there are instances in which the nonlocal invariants really must be included. However, if the original free-energy functional is local—with at most two invariants—and if the coefficient t_{l^*} of the quadratic invariant of the dominant irreducible representation is significantly lower than that of the other l, then only a limited number of nonlocal invariants, say with $l = l^* \pm 1$, may need to be included. A Kim geometrical analysis may remain practical for l larger than 15 and/or 16 but this will need to be verified in future work. It is interesting to note in this context that icosahedral spherical harmonics come in the form of neighboring odd-even pairs of the form of $l:l + 1$, which suggests that this strategy may work for icosahedral ordering for general l as it did for the $l = 15$ and 16 pair.

We have found that, in the case of icosahedral ordering for $l = 15$, the basic tenets of Landau theory can be "saved" at the cost of introducing the nonlocal invariants permitted by the Molien polynomial and generated perturbatively by the entrained contributions of $l = 16$ modes. In actuality, the description of the broken symmetry states directly in terms of multiple irreducible representations is the more economical. The difficulties with "single-l" canonical Landau theory are expected to proliferate for shell structures that require even larger l values. An icosahedral state in the form of, say, a large icosahedral "buckyball" is composed of 20 rounded equilateral triangular facets where particles have sixfold coordination. The same is true for large viral capsids that are constructed by the Caspar-Klug method [21]. These structures are only very poorly represented by any single icosahedral spherical harmonic. It would appear that spherical harmonics are not the best basis set for such cases but it is not clear what would be a better choice.

Other interesting questions await resolution. In the introduction, we discussed that an $(l = 16)$-like icosahedral state is generated by numerical simulations of 72-point particles that were interacting via the LJ pair interaction [4]. The stability range of the icosahedral state is quite small when system parameters such as temperature and interaction range are varied. A variety of other symmetries appear as well (see Fig. 35). The icosahedral state competes with states that have different symmetries: D_{5h}, D_3, tetrahedral, and D_2. The method that we
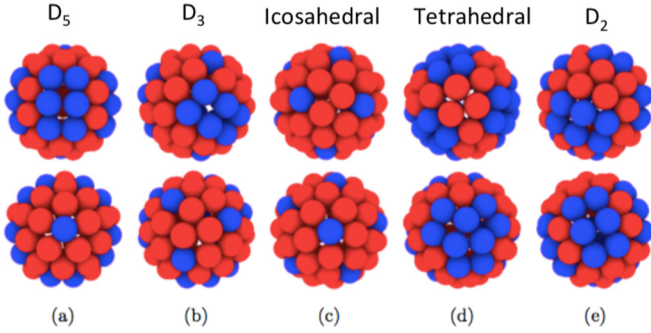
FIG. 35. The five Lennard-Jones packings for $N = 72$ with the lowest potential energy. (a) D_{5h} packing with energy per particle 3.0564 in units of the Lennard-Jones (LJ) binding energy, (b) D_3 packing with 3.0559, (c) icosahedral packing with 3.0548, (d) tetrahedral packing with 3.04636, and (e) baseball symmetry (D_2) with 3.04630. The color indicates the coordination numbers five (blue) or six (red); from Ref. [4].

explored has to account for these other states. We found that in the pure $l = 16$ sector, states with five-, three-, two-, and eightfold symmetry compete with icosahedral symmetry. This is very encouraging but the mirror planes that characterize the D_5, D_3, and D_2 symmetry groups are missing for reasons that are not clear. Higher order invariants may have to be included to explain this.

Chirality is believed to play an important role [6] for the case of viral capsids. The high-temperature symmetry group is SO(3) in this case. Chiral invariants have to be included as part of the expansion. The lowest order chiral invariant is fourth order in the density [5], and it would be interesting to see how this invariant will affect the $l = 15 + 16$ phase diagrams.

We conclude by noting that symmetry arguments play an important role for the design of synthetic molecular shells as exemplified by the work in the Yeates group [22]. It would be interesting to apply the Kim construction method to analyze the symmetry-based strategies developed for shell design.

APPENDIX A: THE QUADRATIC INVARIANT

Given the form of $\rho_l(\theta, \phi)$ in (2.1), the most general form of a quadratic invariant must be

$$\sum_{m=0}^{l} B_m c_{l,m} c_{l,-m} \tag{A1}$$

in order to be unaffected with respect to rotations about the z axis. The next question is what restriction rotational invariance places on the coefficients B_m. We can arrive at that restriction by noting that the generators of rotations about the x or y axis are combinations of angular momentum raising and lowering operators. The raising operator $a^\dagger$ has the following action on the coefficients $c_{l,m}$:

$$a^\dagger c_{l,m} \propto \sqrt{l(l+1) - m(m+1)} c_{l,m+1}. \tag{A2}$$

Consider the two consecutive terms in (A2):

$$B_m c_{l,m} c_{l,-m} + B_{m+1} c_{l,m+1} c_{l,-m-1}. \tag{A3}$$

If we act on these two terms with the operator $\mathbb{1} + \delta a^\dagger$, then two of the $O(\delta)$ terms generated are proportional to

$$\delta \sqrt{l(l+1) - m(m+1)} c_{m+1} c_m (B_m + B_{m+1}). \tag{A4}$$

In order for this to vanish, we must have

$$B_m = -B_{m+1}. \tag{A5}$$

The equality above holds for all $m > 0$. In the case $m = 0$, the same procedure yields

$$B_1 = -2B_0. \tag{A6}$$

Thus, the quadratic invariant must have the form

$$K\left(2\sum_{m=1}^{l}(-1)^l c_{l,m} c_{l,-m} + c_{l,0}^2\right) = K \sum_{m=-l}^{l}(-1)^m c_{l,m} c_{l,-m}. \tag{A7}$$

From the orthonormality of the spherical harmonics and their symmetry properties, this expression is equivalent to

$$K \int \Phi_l(\theta, \phi)^2 \sin\theta \, d\theta d\phi. \tag{A8}$$

It is possible to carry out the same analysis by requiring that the invariant is unchanged under the action of the lowering operator, a. However, given that this is just the Hermitian conjugate of the raising operator, the analysis is fundamentally identical to the one above, leading to exactly the same conclusion.

APPENDIX B: HIGHER ORDER INVARIANTS

The way in which one determines the number of invariants of a particular order is to compare the number of terms that can contribute to an invariant with the number of restrictions on those terms arising from application of the raising operator. At a given order n and angular quantum number l, the invariant is the sum of terms going as

$$B_{m_1,\ldots,m_n} c_{l,m_1} c_{l,m_2} \ldots c_{l,m_n} \delta_{m_1+\cdots+m_n}. \tag{B1}$$

The number of such terms is the number of distinct ways of finding n integers between $-l$ and l that sum to zero. This can be expressed in terms of the number distinct of ways representing the integer $n(l+1)$ as a sum of n positive and nonzero integers less than or equal to $2l + 1$. The restrictions are a set of requirements on terms of the form

$$B'_{m_1,\ldots,m_n} c_{l,m_1} c_{l,m_2} \ldots c_{l,m_n} \delta_{m_1+\cdots+m_n-1} \tag{B2}$$

The number of such terms is the number of distinct ways of finding n integers between $-l$ and l that sum to one. This can be expressed in terms of the number of a way of expressing the integer $n(l+1) + 1$ as a sum of n positive and nonzero integers less than or equal to $2l + 1$. The total number of
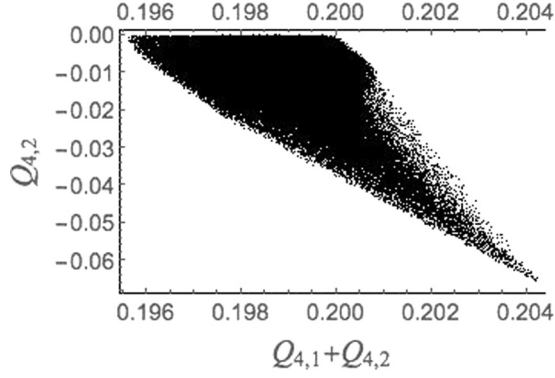
FIG. 36. The portion of the Kim plot in Fig. 6 that corresponds to twofold symmetry, colored black rather than orange, as in Fig. 6. This region is bounded from above by $Q_{4,2} = 0$. The points in the region become sparse in the vicinity of the other boundaries.

distinct nth-order invariants is just the difference between the two numbers above.

Figure 4 shows that difference in the instance of fourth-order invariants, for values of l ranging from 0 to 40. In the case of third-order invariants, the difference is always zero or one: zero for odd values of l and one for even values of l. This is because the only third-order invariant is the integral of the density cubed, and given the symmetry properties of spherical harmonics, such an integral is guaranteed to vanish for odd l. Based on Fig. 4, which also follows from the Molien series [15], it is reasonable to conjecture that that $n_l^{(4)}$ is given by

$$n_l^{(4)} = \left\lfloor \frac{l}{3} \right\rfloor + 1, \tag{B3}$$

where the first term on the right-hand side of (B3) is the largest integer less than or equal to $l/3$.

APPENDIX C: TRACING OUT BOUNDARIES IN THE KIM PLOT

Figure 36 shows the portion of the Kim plot in Fig. 6 corresponding to twofold symmetry. Although the upper boundary of this region at $Q_{4,2} = 0$ is well defined, the other boundaries are somewhat diffuse, especially toward the bottom of the plot, as the points generated by random sampling of the parameters defining the density are sparse in the immediate vicinity of some of the plot's edges. This can be understood heuristically as the consequence of projecting a

high-dimensional region—seven dimensional in this case—onto two dimensions. Consider, for example projecting a collection of uniformly distributed points in a seven-dimensional sphere onto a two-dimensional flat plane. The number of points directly above the plane in the vicinity of the circular surface of the projected sphere will be considerably smaller than the number directly above the center of the circular region into which the points fall.

As an alternative to generating more points, which for large l becomes computationally demanding as well as memory intensive, we adapt the Kim method to trace out the boundary. Recall that minimizing the free energy entails finding the point at which a curve of constant free energy—in the instance of $l = 7$ a straight line—impinges tangentially on the Kim plot. If we were to take all possible orientations for this constant energy surface, we would trace out the convex hull of the Kim plot. Given a different constant free-energy surface, one can perform a more detailed probe of the boundary. To this end, we devise a new surface which, for lack of a better term, we call a "stylus." It is of the general form

$$x \cos \phi + y \sin \phi + K(-x \sin \phi + y \cos \phi - D)^2 = C, \tag{C1}$$

where K, C, and D are constants. For K sufficiently large, this is a very steep parabola. Figure 37 shows the twofold symmetry region and two of the stylus surfaces, for $\phi = 0$ and $K = \pm 5,000$. In practice, we used $K = 10\,000$. We locate the two bounding surfaces by varying D, thus scanning vertically, and determining the minimum value, effectively the quantity C, of the left-hand stylus function and the maximum value of the right-hand one. This process yields the two boundary curves shown in Figs. 6 and 7, as well as the translated versions of those Kim plots.

APPENDIX D: KIM PLOT WITH A CUBIC INVARIANT: DETAILS

The Kim method can also be applied to cases in which third-order invariants arise, as when l is even. Take the instance of a single l system with only one relevant quartic term, say, the local one. The free energy is then

$$\mathcal{F}[\rho_l] = \frac{t}{2}A^2 + \frac{u}{3}A^3 Q_3\{\psi_k\} + \frac{v}{4}A^4 Q_4\{\psi_k\}. \tag{D1}$$

The outcome of minimizing (D1) with respect to A and discarding the possibility of $A = 0$ is

$$\mathcal{F}_{\min} = -\frac{u^4 Q_3^4}{v^3 Q_4^3} \frac{1 + 6(t v Q_4/u^2 Q_3^2)^2 - 6t v Q_4/u^2 Q_3^2 + (1 - 4t v Q_4/u^2 Q_3^2)^{3/2}}{24}$$

$$\equiv -\frac{u^4 Q_3^4}{v^3 Q_4^3} \frac{1 + 6W^2 - 6W + (1 - 4W)^{3/2}}{24}. \tag{D2}$$

From the equations above, we find

$$Q_3^2 = -\frac{t^3}{u^2} \frac{1}{W^3} \frac{1 + 6W^2 - 6W + (1 - 4W)^{3/2}}{24 \mathcal{F}_{\min}}, \tag{D3}$$

$$Q_4 = -\frac{t^2}{v} \frac{1}{W^2} \frac{1 + 6W^2 - 6W + (1 - 4W)^{3/2}}{24 \mathcal{F}_{\min}} = \frac{u^2}{vt} W Q_3^2. \tag{D4}$$
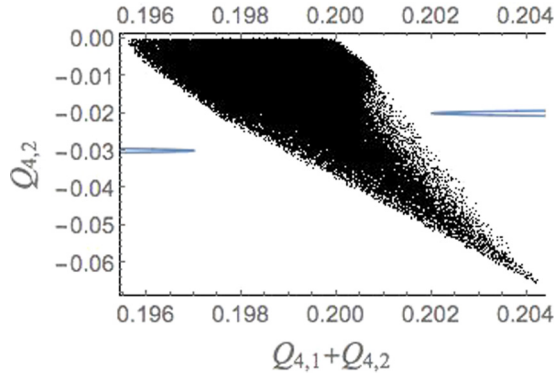
FIG. 37. The twofold symmetry region and two stylus curves.

Both Q_3^2 and Q_4 are positive, the latter to ensure thermodynamic stability. Furthermore, $\mathcal{F}_{\min}$ will be negative. Given this, we see from (D3) and (D4) that the parameter W will have the same sign as t.

The above equations allow us to plot curves of constant free energy in the space spanned by Q_4 and Q_3^2. One important point is that the approach can be generalized to more than one Q_4. If, for instance, there are two quartic invariants, then we replace Q_4 with $aQ_{4,1} + bQ_{4,2}$. The curve defined by (D2) and (D3) becomes a surface in which the Q_4 axis is replaced by lines of constant $aQ_{4,1} + bQ_{4,2}$. This is readily extended to the case of more quartic invariants.

In light of the last line of (D2) and the fact that Q_4, Q_3^2, v, and u^2 are positive, it is clear that the signs of the quantity W and the parameter t must be the same. Given this and the fact that the contribution of the W-dependent expressions to the right-hand sides of (D2) and the first line of (D3) is zero when $W = 2/9$, we can distinguish between two regimes in those equations. The first is $-\infty < W < 0$, which applies when $t < 0$. The second is is $0 < W < 2/9$, appropriate to $t > 0$. Outside of those regimes, the right-hand sides of (D2) and (D3) either apply to the case $\mathcal{F}_{\min} > 0$, which is not of interest, or possess imaginary parts.

The relationships between Q_3^3 and Q^4 are illustrated in Figs. 38 and 39, in which all terms aside from W have been set equal to convenient values.

From these plots—and a bit of analysis—we see that for large amplitudes of the two invariants $Q_3^2 \propto Q_4^{3/2}$. Furthermore, as is evident from the plot, the dependence is monotonic with increasing positive slope. Additionally, inspection reveals that there are three independently adjustable quantities in the two relationships, which can be chosen to be W, $\mathcal{F}_{\min} v/t^2$, and $\mathcal{F}_{\min} u^2/t^3$. This means that we can in principle choose two of those quantities to ensure that a Q_3^2 vs Q_4 curve passes through a given point in the Kim plot. The third quantity can then be chosen so as to adjust the slope of that curve. Given the values of those three quantities,

$$Q_4 = x, \tag{D5}$$

$$Q_3^2 = y, \tag{D6}$$

$$\frac{dQ_3^2}{dQ_4} = s, \tag{D7}$$
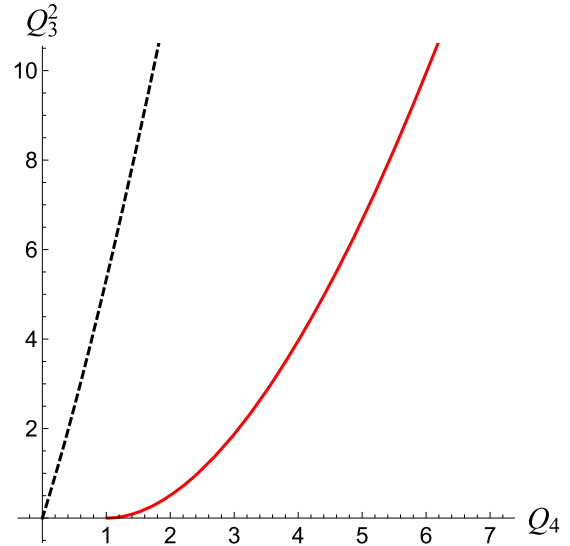
FIG. 38. Plots of Q_3^2 vs Q_4 for values of t that are positive (dashed black curve) and negative (solid red curve). The free energy $\mathcal{F}_{\min}$ has been set equal to $-1/4$, and the parameters u, v, and $|t|$ have been set equal to 1.
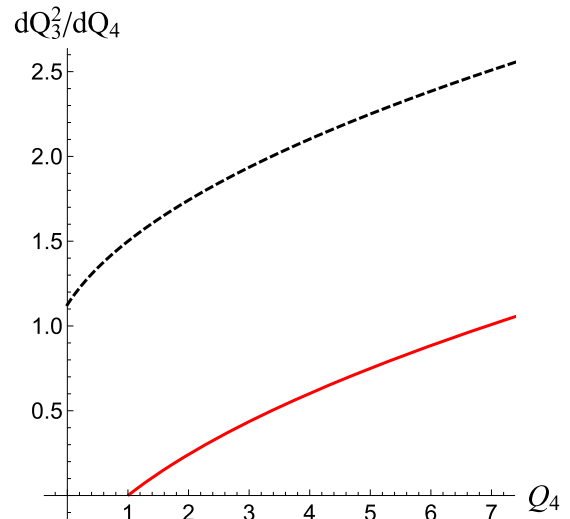
with the additional conditions

$$x > 0, \tag{D8}$$

$$y > 0, \tag{D9}$$

$$s > 0, \tag{D10}$$

we find

$$W = \frac{2sx(3y - 2sx)}{9y^2}. \tag{D11}$$

FIG. 39. The slopes of the curves in Fig. 38, plotted against Q_4. The parameters have been set to the same values as in that figure.
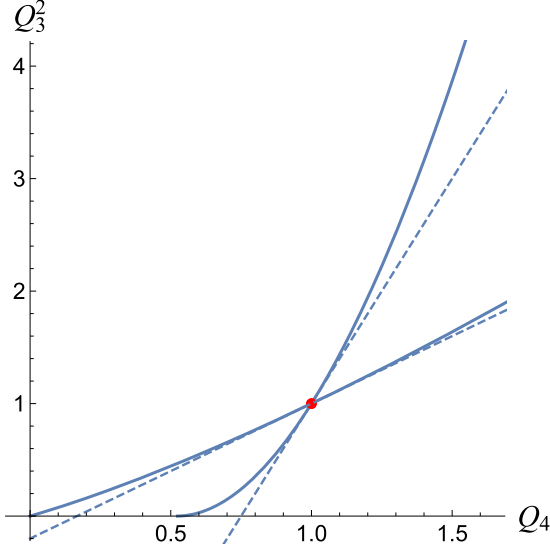
FIG. 40. Two constant free-energy curves passing through the point $Q_4 = 1$, $Q_3^2 = 1$, one with a slope of 1.2, corresponding to a positive value of t, the other with a slope of 4, corresponding to a negative value of t. The dashed lines indicate the slopes.

This result is of interest in the range $s > y/x$. The relationships yield

$$|\mathcal{F}_{\min}| u^2/t^3 = \frac{9y(y - sx)}{2(2sx - 3y)^3}, \tag{D12}$$

$$|\mathcal{F}_{\min}| v/t^2 = \frac{s(sx - y)}{(2sx - 3y)^2}. \tag{D13}$$

Given these equations, it is relatively straightforward to construct the desired constant free-energy curve.

One final point is that the regime $y/x < s < 3y/2x$ corresponds to positive values of t and the regime $s > 3y/2x$ corresponds to negative values of t. Figure 40 displays the results of such a fit, in which two constant free-energy curves have been produced, both going through the point $Q_4 = 1$, $Q_3^2 = 1$, one with a slope of 1.2 and the other with a slope of 4.

Finally, there is the question of the utility of the Kim method with the new free-energy curves, as shown in Figs. 40 and 41, for determining free-energy minima. In order to do this, we need to establish a couple of features of the constant free-energy curves. First, it is clear that two curves for different values of the free energy $\mathcal{F}_{\min}$ will be nonintersecting, as the free energy for fixed values of the coefficients t, v, and u is a single-valued function of the invariants Q_4 and Q_3^2. Next, we note that the slope of a constant free-energy curve is always positive, as indicated in Figs. 38 and 39.

Now, we construct a curve in the parameter space in which the coefficients t, u, and v and the parameter W are kept constant while the free energy $\mathcal{F}_{\min}$ varies. From Eqs. (D3) and (D4), we see that this curve is a straight line with positive slope tv/u^2W. As to the parametric dependence of the invariants on $\mathcal{F}_{\min}$, we calculate the derivative of the right-hand sides of Eqs. (D3) and (D4) with respect to $\mathcal{F}_{\min}$. Given that
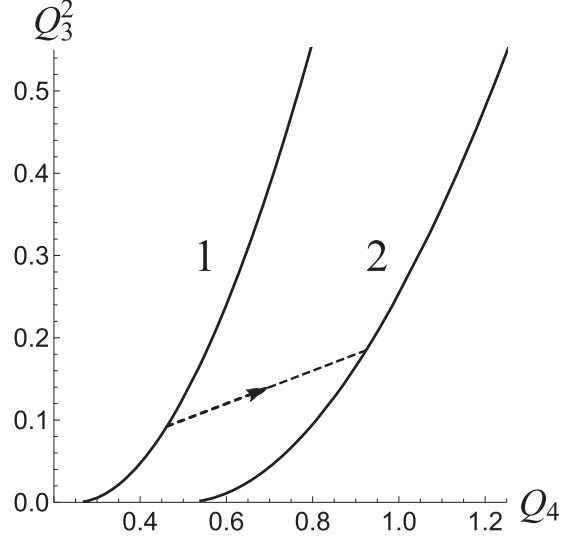

FIG. 41. Two free constant free-energy curves, corresponding to $t = -1$, $u = v = 1$. For curve 1, $\mathcal{F}_{\min} = -1$, while for curve 2, $\mathcal{F}_{\min} = -0.5$. The dashed line joins the points on those two curves for which t, u, and v have the above values, with the parameter W equal to -10 and $\mathcal{F}_{\min}$ varies. The arrow indicates the direction of increasing $\mathcal{F}_{\min}$.

the coefficient t and the variable W have the same sign, and that the numerator $1 + 6W^2 - 6W + (1 - 4W)^{3/2}$ is positive over range $-\infty < W \leqslant 2/9$, which is readily established by inspection, we see that both Q_4 and Q_3^2 increase with increasing $\mathcal{F}_{\min}$. To determine whether displacements along the curve as $\mathcal{F}_{\min}$ increases result in a new constant free-energy curve that is closer to or further way from the origin, we compare the slope of the line element connecting the original and displaced points to the slope of the constant free-energy curve in which the original points lie with the slope of the original free-energy curve. If the slope of the displacement is less than the slope of the constant free-energy curve at the original point, then the displacement connects to a constant free-energy curve that is further away from the origin. If the slope of the displacement is greater than the slope of the free-energy curve at the original point, then it connects to a constant free-energy curve that is closer to the origin. If we call the slope of the original free-energy curve s and the slope of the line element s', we find

$$\frac{s}{s'} - 1 = -\frac{3[2W^2 - 2(\sqrt{1 - 4W} + 2)W + \sqrt{1 - 4W} + 1]}{2[(\sqrt{1 - 4W} + 3)W - \sqrt{1 - 4W} - 1]}. \tag{D14}$$

One can verify by direct evaluation of the right-hand side of (D14) that the difference between the ratio s/s' and 1 is always positive, which means that increasing the free energy $\mathcal{F}_{\min}$ takes the free-energy curve further away from the origin. Given the structure of the Kim plots we consider, this establishes that the Kim method with the new constant free-energy curves does indeed serve to locate global free-energy minima; see Fig. 41 for an illustration of the above argument.

[1] J. D. Honeycutt and H. C. Andersen, J. Phys. Chem. **91**, 4950 (1987).

[2] P. J. Steinhardt, D. R. Nelson, and M. Ronchetti, Phys. Rev. B **28**, 784 (1983).

[3] P. M. Chaikin and T. C. Lubensky, *Principles of Condensed Matter Physics* (Cambridge University Press, Cambridge, UK, 1995).

[4] S. Paquay, H. Kusumaatmaja, D. J. Wales, R. Zandi, and P. van der Schoot, Soft Matter **12**, 5708 (2016).

[5] S. Dharmavaram, F. Xie, W. Klug, J. Rudnick, and R. Bruinsma, Phys. Rev. E **95**, 062402 (2017).

[6] V. L. Lorman and S. B. Rochal, Phys. Rev. B **77**, 224109 (2008).

[7] J. Tsao, M. S. Chapman, M. Agbandje, W. Keller, K. Smith, H. Wu, M. Luo, T. J. Smith, M. G. Rossmann, R. W. Compans *et al.*, Science **251**, 1456 (1991).

[8] V. L. Lorman and S. B. Rochal, Phys. Rev. Lett. **98**, 185502 (2007).

[9] R. Garmann, M. Comas-Garcia, A. Gopal, C. Knobler, and W. Gelbart, J. Mol. Biol. **426**, 1050 (2013).

[10] S. Dharmavaram, F. Xie, W. Klug, J. Rudnick, and R. Bruinsma, Europhys. Lett. **116**, 26002 (2016).

[11] P. C. Matthews, Nonlinearity **16**, 1449 (2003).

[12] M. V. Jarić, Nucl. Phys. B **265**, 647 (1986).

[13] M. V. Jarić, Phys. Rev. Lett. **55**, 607 (1985).

[14] J. S. Kim, Nucl. Phys. B **196**, 285 (1982).

[15] S. Mukai and W. M. Oxbury, *An Introduction to Invariants and Moduli*, Cambridge Studies in Advanced Mathematics (Cambridge University Press, Cambridge, UK, 2003).

[16] See Supplemental Material at http://link.aps.org/supplemental/10.1103/PhysRevE.100.012145 for more information on the physical and mathematical basis of various invariants in the Landau-Brazovskii free energy; the accessibility of symmetry states in the full Kim plot for $l = 6$; the construction of the constant free energy surface for a free energy with quadratic, quartic and sixth order invariants; and the degeneracy properties of some mediated quartic invariants.

[17] E. P. Wigner, *Group Theory and Its Application to the Quantum Mechanics of Atomic Spectra*, Pure and Applied Physics (Academic Press, New York, 1959), p. 372.

[18] S. Alexander and J. McTague, Phys. Rev. Lett. **41**, 702 (1978).

[19] M. O. Lavrentovich, E. M. Horsley, A. Radja, A. M. Sweeney, and R. D. Kamien, Proc. Nat. Acad. Sci. USA **113**, 5189 (2016).

[20] https://drive.google.com/file/d/1DdSuODm3L1DVLH7OW3o Q6iG-7CZNZNZw/view?usp=sharing

[21] D. L. Caspar and A. Klug, Cold Spring Harb. Symp. Quant. Biol. **27**, 1 (1962).

[22] N. P. King, W. Sheffler, M. R. Sawaya, B. S. Vollmar, J. P. Sumida, I. Andre, T. Gonen, T. O. Yeates, and D. Baker, Science **336**, 1171 (2012)